

AD-A127 024

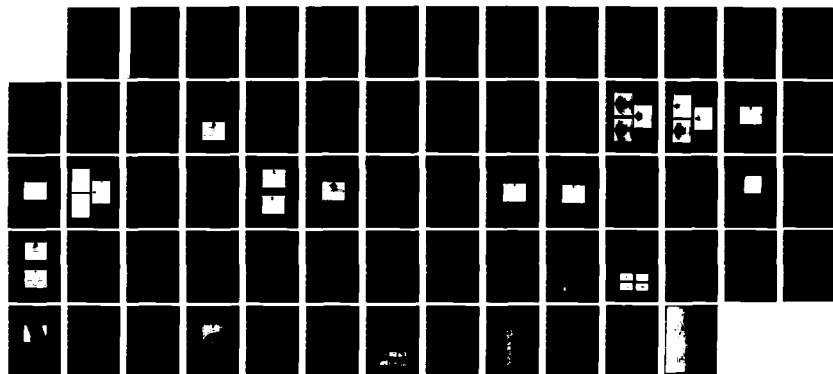
REAL-TIME IMPLEMENTATION OF NONLINEAR OPTICAL  
PROCESSING FUNCTIONS(U) HUGHES RESEARCH LABS MALIBU CA  
B H SOFFER DEC 82 AFOSR-TR-83-0249 F49620-81-C-0086

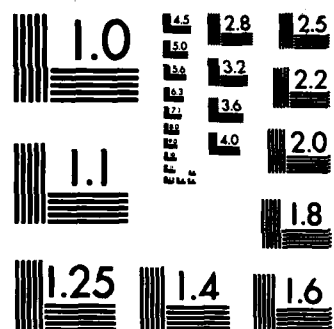
1/1

UNCLASSIFIED

F/G 20/6

NL





MICROCOPY RESOLUTION TEST CHART  
NATIONAL BUREAU OF STANDARDS-1963-A

## REAL-TIME IMPLEMENTATION OF NONLINEAR OPTICAL PROCESSING FUNCTIONS

B. H. Soffer

Hughes Research Laboratories  
3011 Malibu Canyon Road  
Malibu, CA 90265

December 1982

F49620-81-C-0086

Annual Technical Report

15 June 1981 through 15 June 1982

*This manuscript is submitted for publication with the understanding  
that the United States Government is authorized to reproduce and dis-  
tribute reprints for governmental purposes.*

Prepared For

AIR FORCE OFFICE OF SCIENTIFIC RESEARCH

Bolling Air Force Base

Washington, DC 20332



Approved for public release;  
distribution unlimited.

83 04 21 004

DTIC FILE COPY

AD A127022

UNCLASSIFIED

SECURITY CLASSIFICATION OF THIS PAGE (When Data Entered)

REPORT DOCUMENTATION PAGE		READ INSTRUCTIONS BEFORE COMPLETING FORM
1. REPORT NUMBER <b>AFOSR-TR- 88-0249</b>	2. GOVT ACCESSION NO. <b>A127024</b>	3. RECIPIENT'S CATALOG NUMBER
4. TITLE (and Subtitle) <b>Real-Time Implementation of Nonlinear Optical Processing Functions</b>		5. TYPE OF REPORT & PERIOD COVERED <b>Annual Technical Report 15 June 1981 - 15 June 1982</b>
7. AUTHOR(s) <b>B. H. Soffer</b>		6. PERFORMING ORG. REPORT NUMBER
9. PERFORMING ORGANIZATION NAME AND ADDRESS <b>Hughes Research Laboratories 3011 Malibu Canyon Road Malibu, CA 90265</b>		8. CONTRACT OR GRANT NUMBER(s) <b>F49620-81-C-0086</b>
11. CONTROLLING OFFICE NAME AND ADDRESS <b>AFOSR/NE Bolling AFB DC 20332</b>		10. PROGRAM ELEMENT, PROJECT, TASK AREA & WORK UNIT NUMBERS <b>61102F 2305/B1</b>
14. MONITORING AGENCY NAME & ADDRESS (if different from Controlling Office) <b>1</b>		12. REPORT DATE <b>December 1982</b>
		13. NUMBER OF PAGES <b>69</b>
		15. SECURITY CLASS. (of this report) <b>Unclassified</b>
		15a. DECLASSIFICATION/DOWNGRADING SCHEDULE
16. DISTRIBUTION STATEMENT (of this Report)  <b>Approved for public release; distribution unlimited.</b>		
17. DISTRIBUTION STATEMENT (of the abstract entered in Block 20, if different from Report)		
18. SUPPLEMENTARY NOTES <b>Research sponsored by the Air Force Office of Scientific Research (AFSC), under Contract F49620-81-C-0086. The United States Government is authorized to reproduce and distribute reprints for governmental purposes notwithstanding any copyright notation hereon.</b>		
19. KEY WORDS (Continue on reverse side if necessary and identify by block number) <b>Optical signal processing, optical data processing, signal processing, data processing, liquid crystal devices</b>		
20. ABSTRACT (Continue on reverse side if necessary and identify by block number) <b>/ Optical data processing has not yet achieved its potential of increased capacity and speed compared with conventional electronic techniques, primarily for lack of a practical real-time image modulator, and because optical techniques have been almost exclusively limited to linear operations. The continuing research outlined in this report attacks these issues by studying the implementation of real-time nonlinear parallel-processing techniques. The various implementations studied in this program all employed real-time liquid-</b>		

DD FORM 1 JAN 73 1473

EDITION OF 1 NOV 65 IS OBSOLETE  
S/N 0102-LF-014-6601

UNCLASSIFIED

SECURITY CLASSIFICATION OF THIS PAGE (When Data Entered)

UNCLASSIFIED

SECURITY CLASSIFICATION OF THIS PAGE (When Data Entered)

crystal light valves developed and specially modified for these tasks, by Hughes Research Laboratories. One approach we investigated early in the program was to modify and characterize the twisted-nematic liquid-crystal (LC) devices, and then use them in a coherent optical data-processing apparatus using special half-tone screen masks, custom designed for special functions at USC in a cooperative effort under an AFOSR grant. Using the half-tone mask technique, we demonstrated logarithmic nonlinear transformation, permitting us to simplify multiplicative images and perform homomorphic filtering. Furthermore, a novel analog-to-digital converter based on a modified pure birefringence LCLV was developed. It can perform real-time parallel processing using incoherent light, and it promises high data throughput rates. In addition, a novel device that converts light intensity variations to LC grating period variations was fabricated, and is currently being evaluated and improved. This device permits nonlinear functions to be implemented directly without the need for specially made half-tone masks. Besides nonlinear analog functions, this variable grating mode (VGM) device has demonstrated the capability of performing digital optical logic. Logical functions are merely special cases of nonlinearities. In this period we report the behavior of several new VGM LC mixtures. An improvement in response time was noted in some of them. Studies were made of the use of ac and dc to improve the temporal response and a novel technique for spoiling the long-range order has shown a remarkable improvement in response. Finally, some alternatives to the VGM device, which retain the essential optical processing features, are described.

UNCLASSIFIED

SECURITY CLASSIFICATION OF THIS PAGE (When Data Entered)

## TABLE OF CONTENTS

SECTION		PAGE
1	INTRODUCTION . . . . .	7
2	PROGRESS DURING CURRENT YEAR . . . . .	11
	A. New VGM LC Mixtures Studies . . . . .	11
	B. Dynamic Response Studies of VGM Using Application of AC and DC to Improve Response Speed . . . . .	31
	C. Improved VGM Response Speed by Spoiling the Long Range Order . . . . .	38
	D. Alternatives to the VGM Device . . . . .	41
3	PERSONNEL . . . . .	47
4	PUBLICATIONS AND PRESENTATIONS RESULTING FROM AFOSR SUPPORT . . . . .	49
	A. Publications . . . . .	49
	B. Oral Presentations . . . . .	50
APPENDIX	VARIABLE GRATING MODE LIQUID CRYSTAL DEVICE FOR OPTICAL PROCESSING AND COMPUTING . . . . .	53

Accession For		
NTIS GRA&I	<input checked="checked" type="checkbox"/>	
DTIC TAB	<input type="checkbox"/>	
Unannounced	<input type="checkbox"/>	
Justification		
By		
Distribution/		
Availability Codes		
Dist	Avail and/or Special	
A		

AIR FORCE

2000

;

3

6.

1

,

3

100

153501

CH 100-100000 Information Division

3

# LIST OF ILLUSTRATIONS

FIGURE		PAGE
1	Apparatus for studies of the dynamics of the VGM response for various LC mixtures at controlled temperatures . . . . .	13
2	Temporal response of NP-V at 30°C time base: 100 msec/cm, 9 to 18 V-dc cell thickness 8 $\mu$ m . . . . .	17
3	HRL - 2N40 eutectic LC mixture calculations . . . . .	19
4	HRL - 2N42 eutectic LC mixture calculations . . . . .	19
5	HRL new mixture "A" calculations . . . . .	20
6	HRL new mixture "B" calculations . . . . .	20
7	(a) Fast initial temporal response of new HRL VGM LC mixture at 24.8°C . . . . .	24
	(b) Fast initial temporal response of new HRL VGM LC mixture at 40°C . . . . .	25
8	Extended view of temporal response of new HRL LC mixture 1.5 threshold to twice threshold . . . . .	26
9	Temporal response of new HRL VGM LC after 3 hr of continuous use . . . . .	28
10	Temporal response of new HRL VGM LC for various voltage changes . . . . .	29
11	Polarizing microscope picture of typical VGM patterns observed in these experiments . . . . .	30
12	Response before and after 3 hr of continuous use . . . . .	32

FIGURE		PAGE
13	Response time shortening by deliberate switching of the field to zero . . . . .	33
14	Scattered light impulse when switching from 20 to -20 V . . . . .	36
15	Effect of short superimposed dc pulses on VGM efficiency . . . . .	37
16	VGM domains aligned perpendicular to the horizontal 1 $\mu$ m holographic gratings in a 6 $\mu$ m thick cell with 20 V . . . . .	40
17	VGM temporal response +20 to +30 V 1 $\mu$ m grating substrates 500 msec/cm . . . . .	42
18	VGM temporal response +30 to +40 V 1 $\mu$ m grating substrates 2 sec/cm . . . . .	42



## SECTION 1

### INTRODUCTION

Optical data processing (ODP) has promised for two decades a vast increase in processing capacity and speed, compared with conventional electronic techniques. This promise has never been fulfilled for several reasons, most notably because of the lack of a practical real-time image modulator, or light valve, and because optical techniques were almost exclusively limited to linear operations. These restrictions have been removed by the development of the liquid-crystal light valve (LCLV) by Hughes Research Laboratories (HRL), and by nonlinear parallel-processing techniques developed by the University of Southern California (USC). Thus, it is important to determine how successfully nonlinear parallel-processing techniques can be implemented in real time with the various LCLVs.

The implementation and evaluation of these techniques have a direct relationship to current Air Force technology. Pertinent Air Force interests include multidimensional real-time signal and image processing with varied applications, including nonlinear filtering for trajectory control and guidance, "smart" sensing, picture processing, and bandwidth compression. These technologies could benefit substantially from the increased processing capacity and speed that the proposed research may yield.

Section 1 describes nonlinear optical transformation methods and the motivation for studying a real-time application of that technique. The HRL-developed photoactivated twisted-nematic LCLV, the variable grating mode (VGM) LCLV modification and its system configuration for optical processing, and optical logical operation has been described in previous reports. A study of the dynamic performance of the VGM LCLV has been performed, and several new LC mixtures have been prepared to improve the VGM temporal performance. Empirical modeling of the VGM effect has also been performed. Studies were made of the use of ac and dc to improve the temporal response of VGM and work on a novel technique

for spoiling the long-range order to improve response time has begun. Alternatives to the VGM device are also being investigated. The progress made in this period is described in Section 2.

This work has a direct relationship to Air Force interests in the multidirectional processing of real-time signals and images, with applications including nonlinear filtering for guidance and trajectory control, smart sensing, picture processing, and bandwidth compression.

Until now, specified nonlinear operations have been performed only with great difficulty. Coherent optical techniques are essentially restricted to linear operations. Digital processing to produce nonlinear transformations is possible, but only in a slow, serial fashion. Certain nonlinearities can be produced by special photographic techniques, but the speed, accuracy, reproducibility, and dynamic range of these techniques are limited.

We have been pursuing different tasks to attempt to overcome these shortcomings. For the first task we utilized special half-tone screens to modulate the input image, in conjunction with coherent optical processing to desample in the Fourier plane. This technique has made it possible to implement nonlinear effects when higher orders of the half-tone diffraction patterns are examined by spatial filtering. Sawchuk and Dashiell of USC have shown, by using specially fabricated half-tone screens, how a very wide class of two-dimensional point nonlinear functions can be implemented with a large dynamic range as a function of screen design and diffraction order. The nonlinearities can be continuous or discontinuous. Operations such as taking logarithms, exponentiation, level slicing, intensity bandstopping, and histogram equalization can be performed. We have expanded the half-tone screen technique by substituting a real-time photomodulated LCLV for the static photographic recording medium. We have successfully demonstrated a logarithmic nonlinear transformation using this technique. This transformation is useful for homomorphic-filtering applications as we have demonstrated. We, in

cooperation with USC, studied the performance potentials and limitations of this implementation and how to iteratively modify and improve the LCLV and half-tone masks.

A second general method which we are presently studying in this period also overcomes the limitations of serial or photographic processing. It employs, in one realization, an LC effect VGM that, when incorporated into a new type of photoconductive structure, can automatically map image intensity variations into positions in Fourier space. Filtering and reconstructing can then yield many desired nonlinear transformations of the image without the need for specially constructed half-tone masks. A new additional parameter, the intensity, has been made available for processing. Recognizing that digital logical operations are merely a special case of nonlinear operations, we have demonstrated a unique and highly advantageous optical computing scheme using this technique. The VGM device is still in an early stage of development and much material research and device development is still needed to make it into a practical, real-time, reliable optical image modulator. This work is still continuing. Alternative physical realizations of intensity to positional mapping are also being studied.

## SECTION 2

### PROGRESS DURING CURRENT YEAR

During this year, we pursued several tasks for this program which were directed toward further improving our understanding of the VGM effect and toward developing a VGM photoactivated light-valve device. In the VGM effect, certain LC elements exhibit a phase grating whose local period is proportional to the locally applied voltage. When incorporated into a light-valve structure, along with a photoconductive layer, local variations in the spatial distribution of light signal or image intensity are converted into local variations in grating period. In the Fourier transform plane, a new parameter - the intensity - is coded into the spatial distribution in a way that permits great freedom to perform non-linear optical data and image processing, and to perform optical computations as well. In this period, we continued to examine many aspects of the device, including the LC system itself, the temporal dynamic properties of the light valve, including some novel schemes to increase the speed of response, and the detailed optical polarization properties of the VGM diffraction patterns with the goal of modeling the molecular configuration of VGM. We also began to study alternative schemes to the VGM effect wherein the main feature of converting intensity variations to positional variations would be enjoyed along with much faster time-response characteristics.

#### A. NEW VGM LC MIXTURES STUDIES

New VGM LC mixtures of decreased viscosity were prepared and evaluated. The temporal response characteristics proved to be complex and impossible to describe merely with a single set of characteristic rise and decay times. The responses are non-exponential and multi-process with a pronounced memory or hysteresis. There is a slow secular degradation in response. All of these complexities remain to be analyzed. We report some of our

observations illustrating the temporal responses with oscilloscope traces.

Response time measurements of the variable grating mode dynamic behavior using the setup shown in Figure 1 were made to study the effects of LC composition, LC viscosity, cell thickness, applied voltage and temperature on rise and decay times. The measurements were taken on the first order diffracted light from the VGM cell. The diffracted spot of the laser beam was 3 to 5 mm in diameter at the detector 20 cm from the LC plane. The detector was positioned in each experiment at the angle corresponding to the steady-state diffraction angle for the particular field applied. A mask was positioned in front of the detector to give an angular resolution of 1 mm at 20 cm from the VGM cell plane.

Table 1 compares three LC mixtures of different compositions:

2N40 - a mixture of five different alky-alkoxy phenyl benzoates and one alkoxy-alkoxy phenyl benzoate

2N42 - a mixture of five different alkyl-alkoxy phenyl benzoates

NPV - a mixture of azoxy compounds, with a total viscosity range of 25 to 47 cP.

A cell thickness of 7.5  $\mu\text{m}$  and a temperature of 25°C were kept constant for the comparison. With an applied dc signal 2 times the threshold voltage, the viscosity effect can be noted. The lower viscosity 2N42 mixture has an "on" time (delay time plus rise time), more than 2 times faster while the decay time is similar to that of 2N40. The azoxy compounds in NPV have the lowest viscosity with fastest turn on time and a slightly slower decay time. Unfortunately, as indicated by the decrease of resistivity after 16 hours of testing, this mixture is less stable than the ester type LCs.

The cell thickness effect on the VGM response time was tested in the 2N42 LC mixture. A 4.3  $\mu\text{m}$  thickness cell was fabricated on optical flats with a  $\text{SiO}_x$  spacer. In this particular cell the first-order diffraction was very weak, whereas the second order was much stronger. Detailed examination of the cell explained this phenomenon since the counterelectrode had a defective

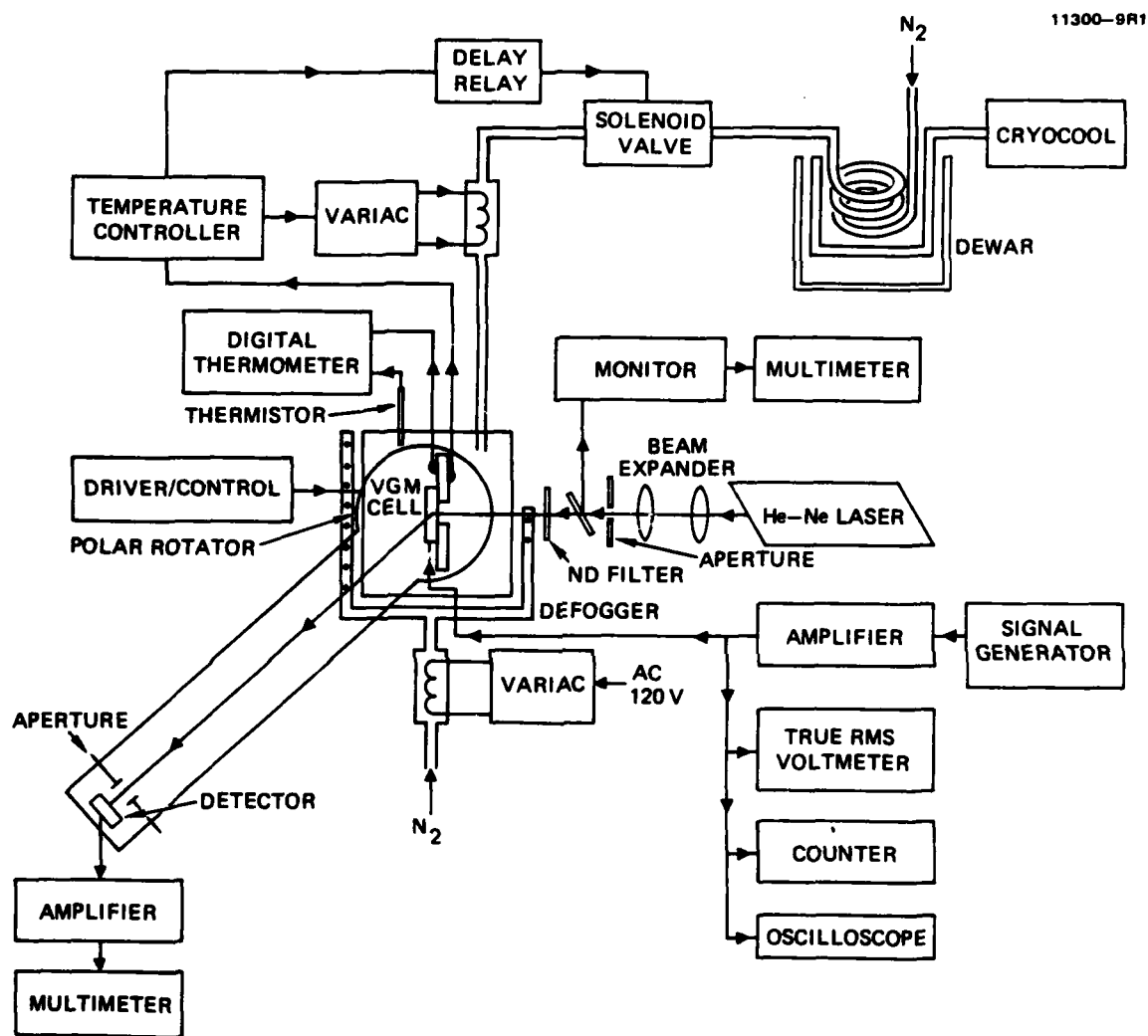


Figure 1. Apparatus for studies of the dynamics of the VGM response for various LC mixtures at controlled temperatures.

Table 1. VGM Response Time Measurements

LC <sup>a</sup> 7.5 $\mu\text{m}$	Threshold Voltage, V	Resistivity, <sup>b</sup> $\rho_1, \Omega \text{ cm}$	Signal, Vdc	Initial				After 16 hrs DC			
				Delay time, <sup>c</sup> msec	Rise time, <sup>d</sup> msec	Decay time, <sup>e</sup> msec		Delay time, <sup>c</sup> msec	Rise time, <sup>d</sup> msec	Decay time, <sup>e</sup> msec	Resistivity, $\rho_1, \Omega \text{ cm}$
2N40 $\eta = 46.9 \text{ cP}$	15	$4.9 \times 10^{10}$	0 $\rightarrow$ 30	480	1400	200		380	400	13	$2.4 \times 10^{10}$
			15 $\rightarrow$ 30	450	850	50		440	450	42	
2N40 $\eta = 46.9 \text{ cP}$	15	$3.9 \times 10^{10}$	0 $\rightarrow$ 30	400	640	15		360	580	16	$1.2 \times 10^{11}$
			15 $\rightarrow$ 30	440	510	48		490	490	44	
			+AC(f) { 0 $\rightarrow$ 30 15 $\rightarrow$ 30	390	630	16		400	560	18	
				480	580	44		540	480	42	
2N42 $\eta = 32.6 \text{ cP}$	10	$1.5 \times 10^{10}$	0 $\rightarrow$ 20	210	210	19		240	230	17	$1.8 \times 10^{10}$
			10 $\rightarrow$ 20	215	210	58		.185	135	82	
Merck NPV $\eta = 24.9 \text{ cP}$	10	$1.2 \times 10^{10}$	0 $\rightarrow$ 20	180	420	20		160	520	26	$8.3 \times 10^9$
			10 $\rightarrow$ 20	150	120	100		130	220	148	

a. LCs tested at 25°C in cell fabricated from ITO/PVA coated optical flats with 7.5 micron SiO<sub>x</sub> spacers, rubbed for parallel alignment.

b. Resistivity measured with 0.1 V 100 Hz sine wave signal.

c. Delay time measured from start of signal to 10% of total light transmission in 1st order defraction.

d. Rise time measured between 10% and 90% of the total light transmission in 1st order defraction.

e. Decay time measured from 90% of 1st order defraction after signal was turned off.

f. Superimposed ac signal of 4.3 Vrms sine wave at 40 kHz.

antireflection (AR) type coating on the outer surface acting as a crossed polarizer, extinguishing odd numbered diffraction orders. The 4.3  $\mu\text{m}$  thickness cell of 2N42 LC was remade using a different counterelectrode, and normal VGM behavior was observed. It is difficult to compare response time versus cell thickness since the thicker cells need longer time to activate as can be seen in Table 2. However, it is seen that the thickness effect on turn-on response time is similar in VGM operation to other types of LC operations. The thinner the cell, the faster the turn-on time. The decay times observed in the above data do not follow the same relationship. A small increase in temperature lowers the diffraction efficiency and slows down the turn-on time. By increasing the temperature, the 2N42 viscosity has indeed been lowered.\* However, the response time seems to be controlled by other parameters, in addition to viscosity, such as the elastic constants and dielectric constants. The dielectric constants and the dielectric anisotropy of mixture 2N42 have been studied,\* as a function of temperature, and  $\Delta\epsilon$  becomes more negative between 15°C and 45°C. We have established that LC mixtures with large negative  $\Delta\epsilon$  do not exhibit the VGM effect.

The temperature and the cell-thickness effects were tested with a second LC mixture of different composition, the azoxy compounds of Merch NPV. Two cells were fabricated on optical flats using an 8  $\mu\text{m}$   $\text{SiO}_x$  spacer for the thicker cell and a 3.6  $\mu\text{m}$  mylar spacer for the thinner cell. Parallel alignment, in both cases, was achieved by overcoating the ITO with PVA and rubbing for uniform direction. Diffraction efficiency was also monitored in these tests by measuring the photodetector output in arbitrary millivolt units. Table 3 summarizes the signals used in the corresponding response times that were obtained.

---

\*J.D. Margerum, J.E. Jensen, and A.M. Lackner, "Effects of Molecular Length on Nematic Mixtures," *Mol. Cryst. Liq. Cryst.* 68, 137-156, 1981.



Table 2. Effect of Cell Thickness

LC	Cell Thickness, $\mu\text{m}$	Temperature, $^{\circ}\text{C}$	Signal V-dc	On/Off Interval Half Period	Activation Delay Time, msec	Rise Time, msec	Decay Time, msec
2N42	7.5	24.8	10 to 20	1 sec	215	210	58
2N42	4.3	25.7	9 to 18	200 msec	30	70	110
2N42	4.3	25.7	9 to 18	100 msec	20	55	75
2N42	4.3	30.0	9 to 18	200 msec	50	100	85

Table 3. Effect of Cell Thickness  
Np V LC Studies

Cell Thickness, $\mu\text{m}$	Temperature, $^{\circ}\text{C}$	Relative Diffraction Strength, mv	Signal, V-dc	On/Off Interval Half Period, msec	Delay Time, msec	Rise Time, msec	Delay Time, msec
8.0	25.8	38	9.0 to 18.0	500	100	80	160
3.6	24.8	62	9.0 to 20.0	100	20	30	40
	24.8	53	9.0 to 18.0	100	24	36	38
	29.9	44	9.0 to 18.0	100	24	30	30
	35.0	33	9.0 to 18.0	100	24	26	26
	24.8	38	9.0 to 18.0	500	95	185	17
	24.8	30	9.0 to 18.0	200	85	75	15
	24.8	39	9.0 to 18.0	100	38	52	35
	24.8	26	9.0 to 18.0	50	14	32	28

Comparing the response time of the 8.0 and 3.6  $\mu\text{m}$  cells using a 500 msec ON/OFF signal shows small increase in turn-on time as we go to thinner cells; however, the decay time showed a reduction of an order of magnitude. But in the 3.6  $\mu\text{m}$  cell the signal period was cut to 100 msec, without reducing diffraction efficiency, and the response time was reduced to 60 msec on-time, 38 msec decay time, or (as measured two days later) 90 msec on-time and 35 msec decay time. Both of these times are close to real-time device operation rates. But this fast response is for a very special circumstance, i.e., going from just below threshold to twice threshold. The memory of the grating pattern may persist below threshold making its reformation a much faster process. The temperature effect on the NPV LC is similar to that observed with HRL-2N42; i.e., at higher temperatures the diffraction efficiency is much lower.

When the 8.0- $\mu\text{m}$ -thick cell was operated at an elevated temperature of 30°C, the diffraction brightness was decreasing (three scans within 3 min of signal, 500 msec ON/OFF) while a curious spike was created in the decay cycle (see Figure 2).

11641-2

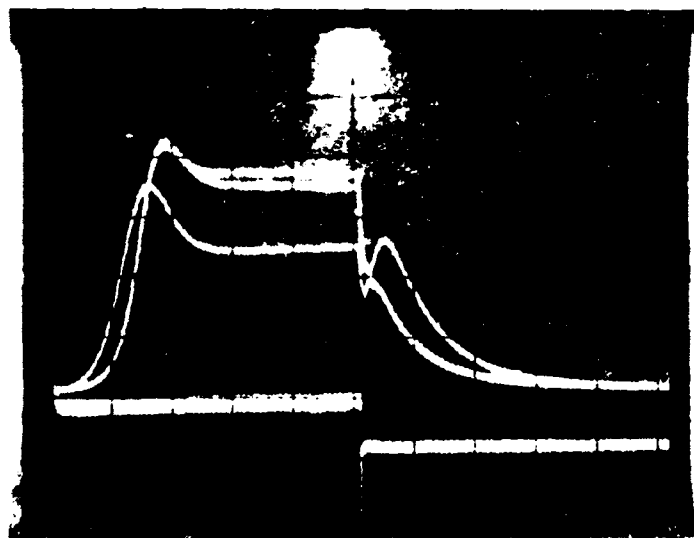
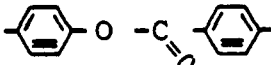


Figure 2. Temporal response of NP-V at 30°C  
time base: 100 msec/cm, 9 to 13 V-dc  
cell thickness 8  $\mu\text{m}$ .

In our internal LC research program we have developed a computer program for predicting the properties of multicomponent eutectic mixtures. By studying the effect of LC structure on viscosity and anisotropy, and assigning class viscosity and class anisotropy values to each component, we revised our computer program to calculate the eutectic mixture with the average molecular length, viscosity, dielectric anisotropy, as well as the melting point and clear-point of the mixture. This is done by utilizing the values of length,  $\eta_{\text{class}}$ , and  $\Delta\epsilon_{\text{class}}$  for each component. Examples of the computer printout for two old eutectic mixtures are shown in Figures 3 and 4. The input data are the compound code, its melting point (MP), clearpoint (CLPT), molar heat of fusion (HF), molecular length (MLEN), molecular weight (MWT), class viscosity (VISC), and class dielectric anisotropy (DEL). All of this information is stored in the system for each component. The calculated output data are the mole fraction (XI) and weight percent (Wt.%) of each component in the eutectic mixture and the melting point, clearpoint, length, viscosity, and dielectric anisotropy of the mixture. This computer program greatly facilitates the process of seeking new mixtures that are likely to have desired values of nematic temperature range, viscosity, and dielectric anisotropy for any LC applications.

Each of the new VGM mixtures calculated in Figures 5 and 6 shows considerably lower viscosity than the two ester mixtures, 2N40 and 2N42, which we have previously studied. The dielectric anisotropy of the new mixtures, A and B, are not correct dielectric anisotropy. However, these mixtures can be slightly altered from eutectic to obtain the needed  $\Delta\epsilon$  by adding some positive  $\Delta\epsilon$  component or reducing the percentage of the positive material. For example, mixture A in Figure 5 has a calculated  $\Delta\epsilon$  of -0.94, but a very low viscosity of 22.89 cP. The eutectic mixture was prepared according to the computer calculation and the dielectric anisotropy was changed by adding a highly positive anisotropy ester component such as CN  C<sub>5</sub>H<sub>11</sub> (NC - (C)5).

TEST.VGM:4

23-NOV-1981 14:01:31.62

Page 1

#	COMPOUND	MP	CLPT	HF	LEN	XI	MWT	WT%	VISC	DEL
1	10-1	96.20	10.00	7197.	16.20	0.0614	242.28	4.67	36.00	-0.25
2	20-3	75.70	68.00	6716.	19.67	0.1267	284.36	11.31	36.00	-0.25
3	20-5	62.80	63.00	7492.	22.21	0.1511	312.41	14.82	36.00	-0.25
4	40-1	72.90	53.00	7808.	19.61	0.0992	284.36	8.85	36.00	-0.25
5	40-6	40.00	49.00	8424.	25.81	0.2993	354.49	33.31	36.00	-0.25
6	60-01	54.90	77.40	6189.	23.60	0.2624	328.41	27.05	82.00	-0.05

MIXTURE MELTING POINT= 14.382

MIXTURE CLEAR POINT= 58.976

MIXTURE LENGTH= 22.70

MIXTURE VISCOSITY= 48.07

MIXTURE DIELECTRIC ANISOTROPY= -0.20

Figure 3. HRL - 2N40 eutectic LC mixture calculations.

VGM.101:1

15-DEC-1981 10:29:55.39

Page 1

#	COMPOUND	MP	CLPT	HF	LEN	XI	MWT	WT%	VISC	DEL
1	10-1	96.20	10.00	7197.	16.20	0.1122	242.28	9.28	36.00	-0.25
2	20-3	75.70	68.00	6716.	19.67	0.2224	284.36	21.59	36.00	-0.25
3	20-5	62.80	63.00	7492.	22.21	0.2831	312.41	30.19	36.00	-0.25
4	40-1	72.90	53.00	7808.	19.61	0.1908	284.36	18.52	36.00	-0.25
5	40-3	70.70	61.00	8150.	21.78	0.1914	312.41	20.41	36.00	-0.25

MIXTURE MELTING POINT= 28.846

MIXTURE CLEAR POINT= 55.873

MIXTURE LENGTH= 20.39

MIXTURE VISCOSITY= 36.00

MIXTURE DIELECTRIC ANISOTROPY= -0.25

Figure 4. HRL - 2N42 eutectic LC mixture calculations.

VGM.101110 Mixture A

15-DEC-1981 10:29:34.74

Page 1

#	COMPOUND	MP	CLPT	HF	LEN	XI	MWT	WTX	VISC	DEL
1	10-1	96.20	10.00	7197.	16.20	0.0401	242.28	3.25	36.00	-0.25
2	20-3	75.70	66.00	6716.	19.67	0.0851	284.36	8.09	36.00	-0.25
3	20-5	62.80	63.00	7492.	22.21	0.0970	312.41	10.13	36.00	-0.25
4	40-1	72.90	53.00	7808.	19.61	0.0625	284.36	5.94	36.00	-0.25
5	40-3	70.70	61.00	8150.	21.78	0.0597	312.41	6.23	36.00	-0.25
6	10-C5	40.90	71.30	5098.	21.40	0.1481	304.43	35.44	16.00	-1.30
7	20-C5	49.00	79.80	6598.	20.21	0.1956	290.40	19.00	16.00	-1.30
8	20-C5	56.90	85.90	7692.	22.59	0.1119	318.46	11.92	16.00	-1.30

MIXTURE MELTING POINT= 4.976

MIXTURE CLEAR POINT= 69.296

MIXTURE LENGTH= 20.93

MIXTURE VISCOSITY= 22.89

MIXTURE DIELECTRIC ANISOTROPY= -0.94

Figure 5. HRL new mixture "A" calculations.

VGM.101111

15-DEC-1981 10:29:32.56

Page 1

#	COMPOUND	MP	CLPT	HF	LEN	XI	MWT	WTX	VISC	DEL
1	40-1	72.90	53.00	7808.	19.61	0.0170	284.36	1.57	36.00	-0.25
2	40-3	70.70	61.00	8150.	21.78	0.0153	312.41	1.49	36.00	-0.25
3	10-C5	40.90	71.30	5098.	21.40	0.1488	304.43	14.11	16.00	-1.30
4	20-C3	49.00	79.80	6598.	20.21	0.0651	290.40	5.88	16.00	-1.30
5	40-C4	40.50	70.00	4188.	23.84	0.2109	332.49	21.84	16.00	-1.30
6	60-C4	26.00	70.00	5360.	26.15	0.2070	360.54	23.24	16.00	-1.30
7	60-C5	32.20	79.80	5056.	27.41	0.1904	374.57	22.21	16.00	-1.30
8	7YPCN	30.00	57.00	6100.	0.00	0.1100	283.50	9.71	27.00	8.40

MIXTURE MELTING POINT=-18.485

MIXTURE CLEAR POINT= 70.380

MIXTURE LENGTH= 20.83

MIXTURE VISCOSITY= 18.25

MIXTURE DIELECTRIC ANISOTROPY= 0.14

Figure 6. HRL new mixture "B" calculations.

Table 4 shows new compositions tested for VGM. The new mixture B in Figure 6 is not a eutectic composition.

Of the eight mixtures in Table 4, only one showed VGM domains with dc signals, namely, mixture B with 5.1% NC - (C)5. Mixtures with somewhat higher, 5.7% additive or slightly lower 4.4%, additive concentration were already too positive or too negative in anisotropy, respectively. The addition of 5.1% NC-(C)5 did not increase the viscosity of mixture B (estimated to be 22.6 cP), while the dielectric anisotropy should be close to -0.1. This new LC mixture was tested for VGM response time using a test cell of optical flats with ITO/PVA coating and a 3.6  $\mu$ m mylar spacer. Alignment is achieved by parallel rubbing of the PVA. All the collected response time data are summarized in Table 5. Typical oscilloscope traces of the temporal response are shown in Figure 7. This new VGM mixture shows several advantages over the previously tested 2N42 or NP V. Since it is a mixture of esters only, it is colorless and more stable than the commercial Merck NP V. Increasing the temperature of the LC in the test device does not lower the diffraction efficiency and speeds up response times, both the turn-on and delay times. Using 100 msec ON and 100 msec OFF square-wave dc signals at 2x threshold voltage results in fast enough response at any of the above temperatures for some special real-time device applications.

Using our new low-viscosity VGM LC we conducted a series of VGM response-time experiments for a variety of voltage changes and switching periods. We measured the time required for a diffracted spot to shift to a new position (angle change) as a result of a change in the field applied to the cell.

The test cell used in these tests was filled with the newly prepared low viscosity LC mixture A described above. The K1720-143B test cell was 3.6  $\mu$ m thick. As before, the first-order diffracted spot of the laser beam was 3 to 5 mm in diameter at 20 cm from the cell LC plane.

Table 4. Properties of New VGM LC Mixtures

Mixture Sample	% NC - (C)5	Resistivity	$\Delta\epsilon$	VGM	Remarks
A	—	$2.54 \times 10^{11}$	-0.94	No	At 100 Vdc
B	5.1	$2.12 \times 10^{11}$	-	Yes	$V_{th} = 17$ Vdc
C	2.5	$1.81 \times 10^{11}$	-	No	At 100 Vdc
D	10.0	$2.54 \times 10^{11}$	+	No	Color shift at 5V
E	3.5	$2.54 \times 10^{11}$	-	No	At 140 Vdc
F	4.4	$2.54 \times 10^{11}$	-	No	At 100 Vdc
G	7.2	$1.81 \times 10^{11}$	+	No	Color shift
H	5.7	$2.54 \times 10^{11}$	$0 \rightarrow +$	No	Color shift

These data were taken with photocell detectors placed at the appropriate angle of diffraction that corresponded to the steady-state value with the field applied. The detectors were masked as before give a detector-angular resolution of 1 mm at 20 cm from the cell plane. Figure 8 illustrates the case where the field is switched from 25.5 V ( $1.5 \times V_{th}$ ) to 34 V ( $2 \times V_{th}$ ) at 10-sec intervals (20-sec period). The top trace measures the diffraction intensity at the 34-V position, while the bottom trace measures it at the 25.5-V position. The rapid times observed in Figure 7 can be noted in these pictures after each fiducial mark. The longer time constants — 10% to 90% and 90% to 10% — are approximately 5 sec in this experiment. It is important to emphasize that the top trace is the photocell output from the 34-V steady-state diffraction angle position, the center trace is the fiducial marker pulse from the dc voltage program generator, and

Table 5. Response Time of New VGM LC Mixture

Temperature, °C	Arbitrary Diffraction Strength, mV	Signal, V-dc	On/Off Interval msec	Delay Time, msec	Rise Time, msec	Decay Time, msec
24.8	215	17.0 - 34.0	1000	60	240	70
	230		500	50	60	90
	230		200	20	40	75
	220		100	10	34	56
	190		50	4	30	36
29.9	260	17.0 - 34.0	200	20	30	55
	250		100	8	28	48
	225		50	4	24	32
34.9	230	17.0 - 34.0	200	20	20	55
	230		100	8	20	48
	210		50	4	18	32
40.0	240	17.0 - 34.0	200	20	15	55
	240		100	7	24	42
	210		50	4	14	30



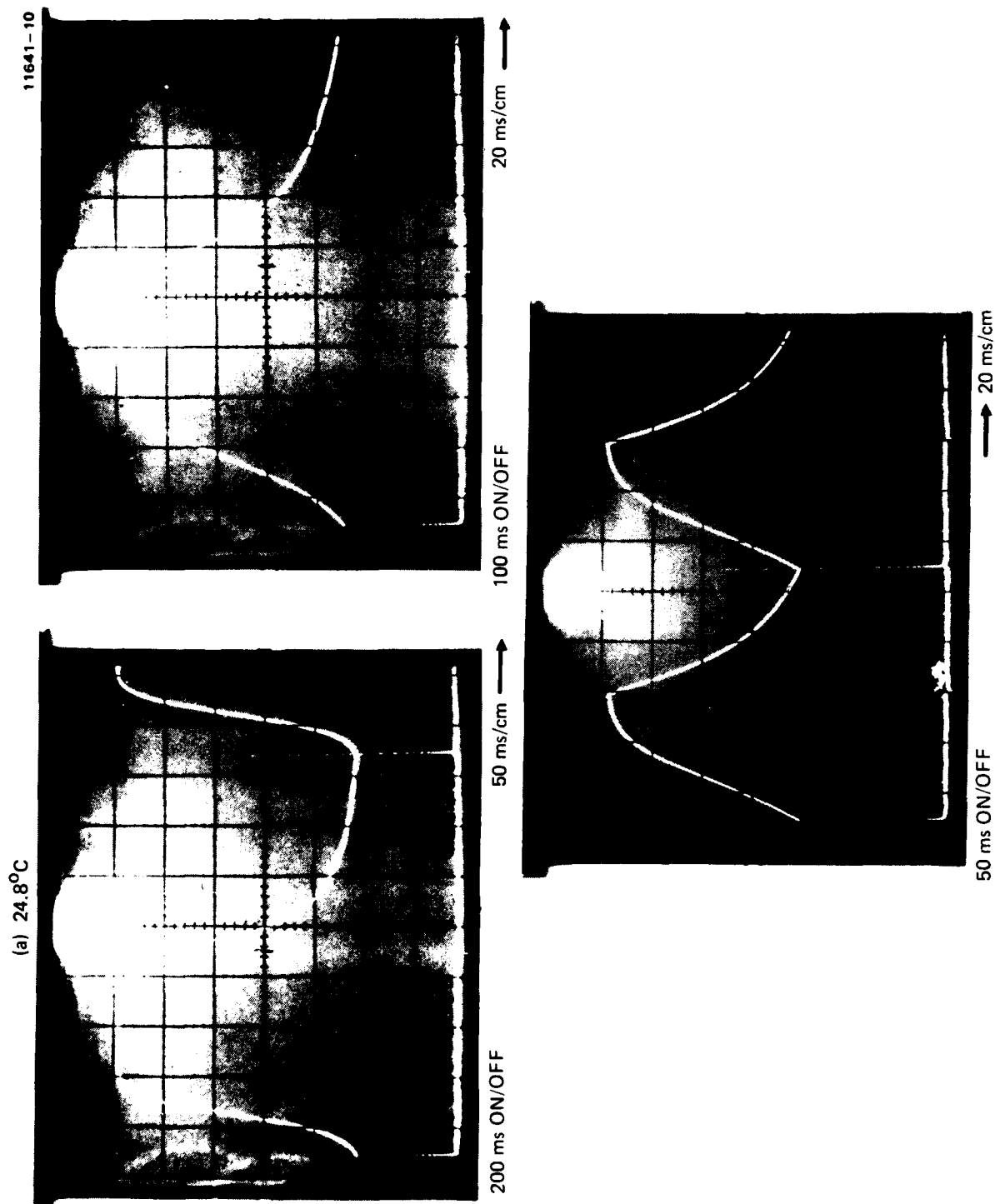


Figure 7(a). Fast initial temporal response of new HRL VGM LC mixture at 24.8°C.

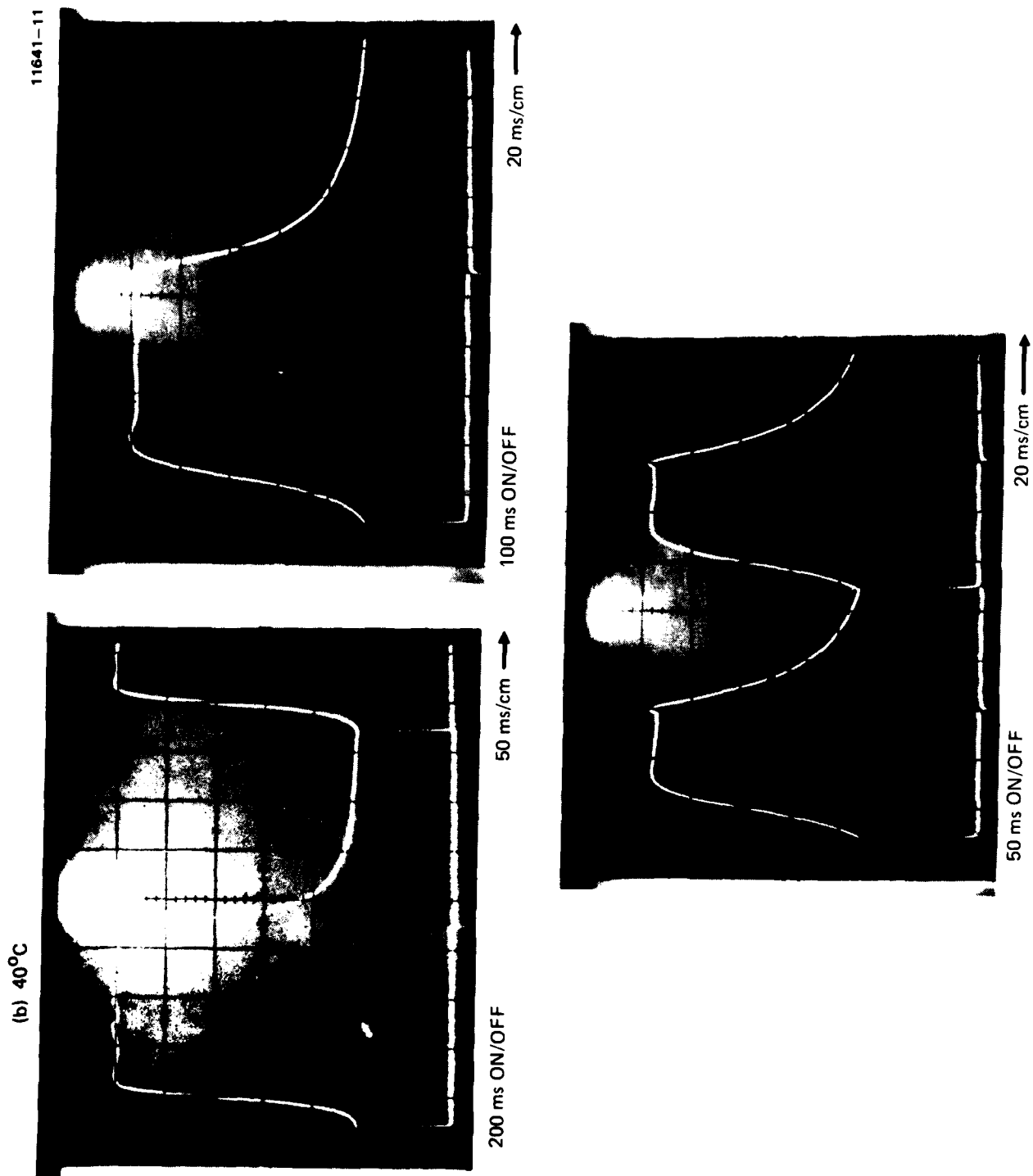
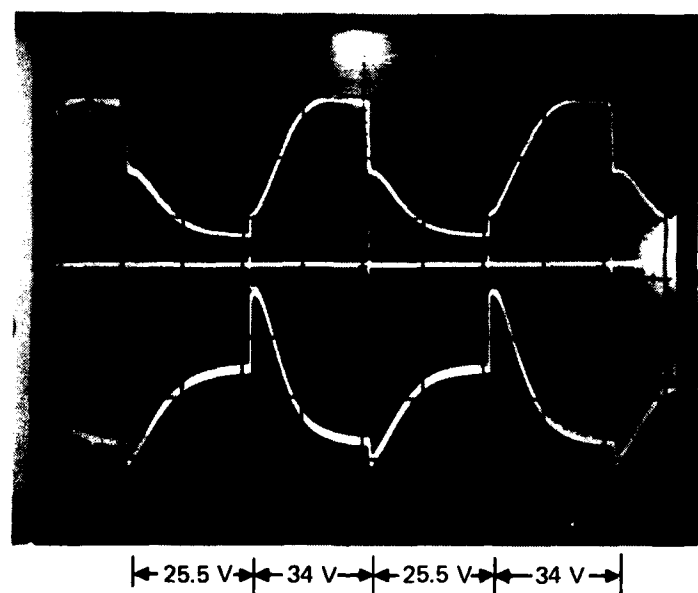


Figure 7(b). Fast initial temporal response of new HRL VGM LC mixture at 40°C.

11641-9



TIME BASE 5 sec/cm

TOP TRACE: 34 V DIFFRACTION POSITION DETECTOR

BOTTOM TRACE: 25.5 V DIFFRACTION POSITION DETECTOR

CENTER TRACE IS THE FIDUCIAL MARKER

Figure 8. Extended view of temporal response of new HRL LC mixture 1.5 threshold to twice threshold.

the bottom trace is the photocell output from the 25.5-V steady-state diffraction angle position. The fast portion of the traces immediately following each marker pulse is the very rapid change in intensity that occurs before the diffraction spot begins to move and to fully form in its new position. This initial impulsive response is not yet understood.

The traces in Figure 9 are taken under the same conditions as was Figure 8, but several hours later. The response has obviously slowed, the diffraction angle has changed slightly, and the intense portion of the diffracted spot is sweeping slightly past the detector centerline making precise time measurements impossible. This characteristic change with hours of use is also present in the following series of photographs, which shows relative angle changes and time of response for different sets of field applied.

Figures 10(a), (b), and (c) show the relative response times and amplitudes for a series of field changes. The fully cycle time used here is 40 sec/cycle. The high field detector (top trace) is repositioned in each figure to correspond to the steady-state angle required. In Figure 10(a) the high voltage diffraction, after an essentially zero "delay," has a 10 to 90% rise time of 17 sec, and decay time of 2 sec. The low-voltage diffraction has a 4 sec rise and 6 sec decay with essentially no delay.

In Figure 10(b), going from 25.5 V to 32 V, cyclically, we note the high voltage rise time to be 15 sec and decay time to be 5 sec; the low voltage rise time is greater than 7 sec (not equilibrium) and the decay time is 10 sec. The delay time is still negligible.

In Figure 10(c), going from 25.5 V to 30 V, the rise time of the higher voltage diffraction is greater than 20 sec and the decay time is 17 sec. The lower voltage diffraction has a rise time of greater than 5 sec and decay time of approximately 12 sec.

The quality of the VGM is quite good in this series of experiments as can be seen from Figures 11(a) and (b), where the VGM was viewed in the polarizing microscope in steady-state condition at comparable field conditions.

11641-8

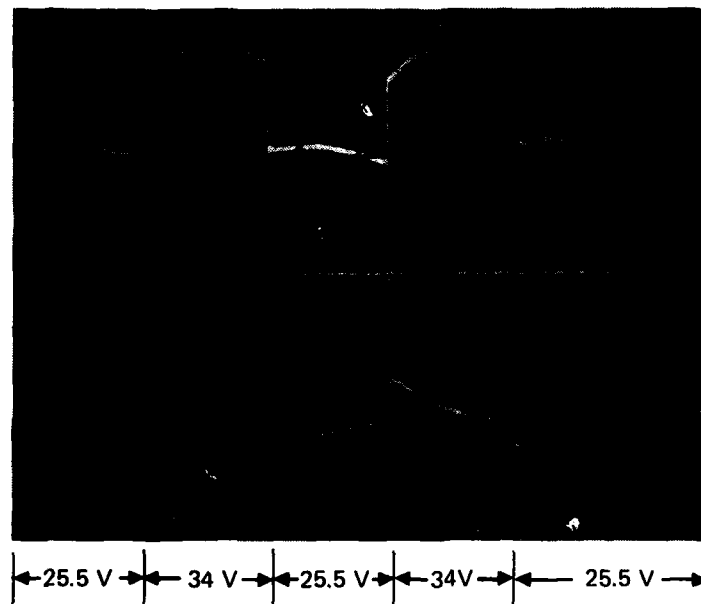


Figure 9. Temporal response of new HRL VGM LC after 3 hr of continuous use.

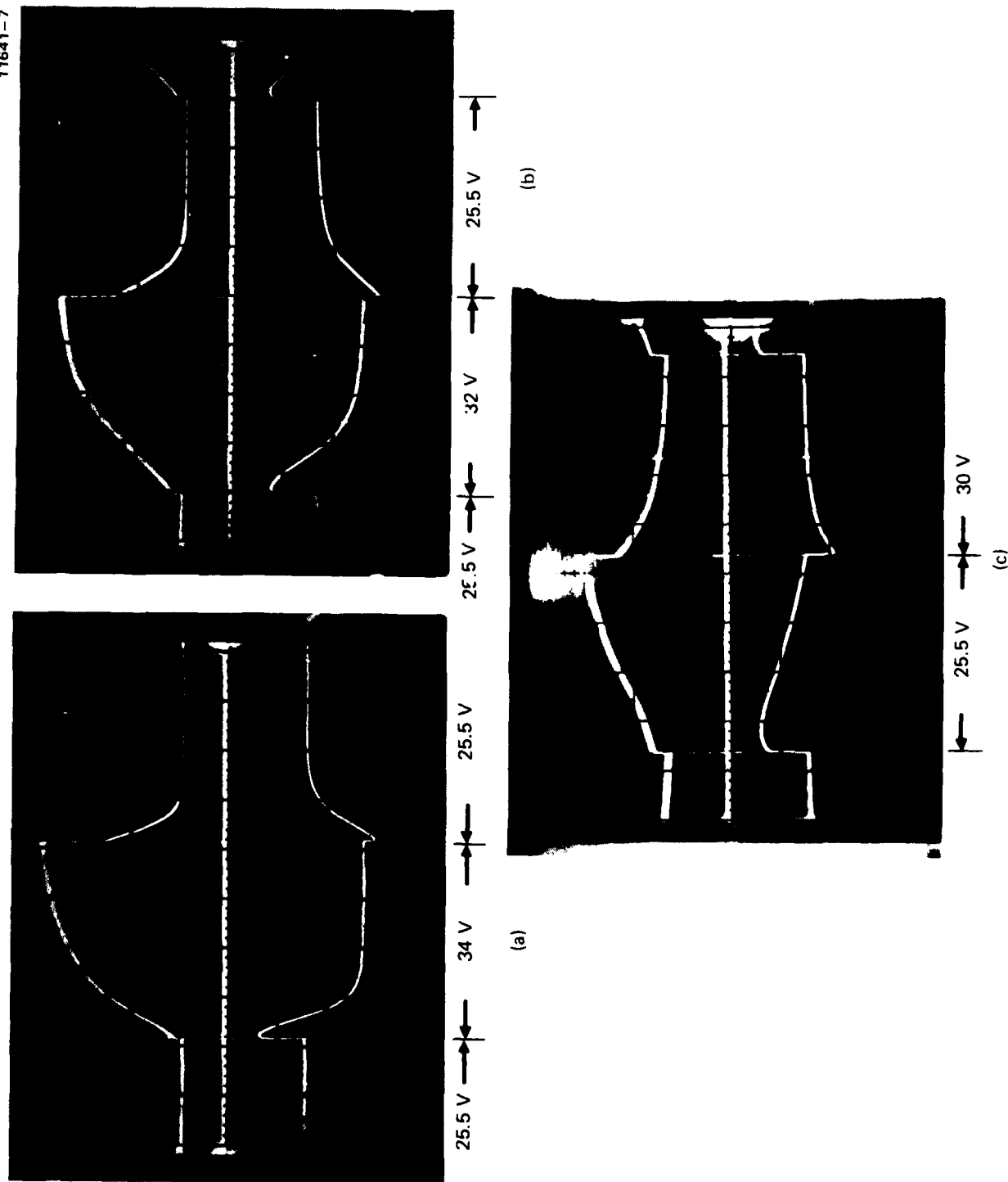
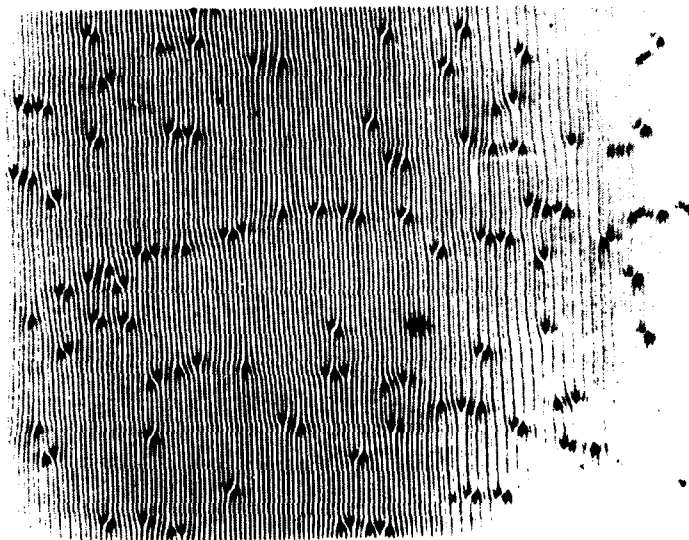
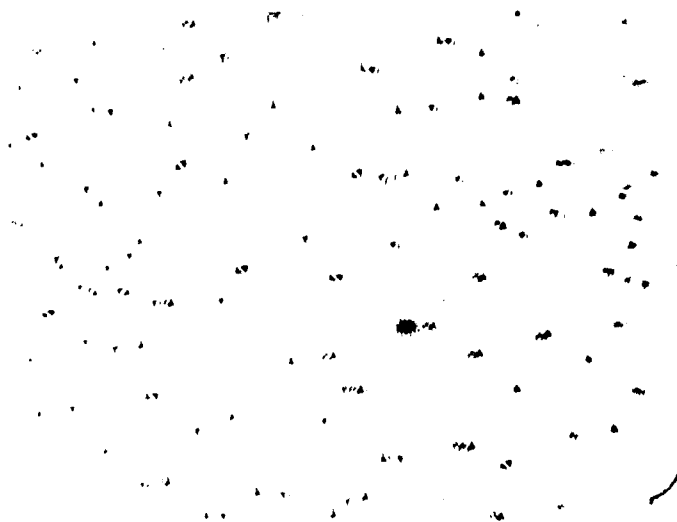


Figure 10. Temporal response of new HRL VGM LC for various voltage changes. Top trace: High voltage diffraction. Bottom trace: Low voltage diffraction. Center Trace: Fiducial marker (5 sec/cm).



(a) 25.5 Vdc



(b) 34 Vdc

Figure 11. Polarizing microscope picture of typical VGM patterns observed in these experiments.

The breaks in the grating lines are the points at which a new line is adding-in on increased field, or an old line subtracting-out on decreased field.

We have determined that this process seems to become slower when the cell is continuously cycled for several hours. Figure 12(a) shows typical initial response when using a 40 sec cycle time. The rise and decay times are greater than 15 sec. After continuous cycling for 3 hr the response is considerably slower, as shown in Figure 12(b).

We then found that this tendency to become slower with continuous use could be reversed by switching the field to zero at the start of each cycle! As can be seen in Figure 13, the speed of response is greatly increased, even though this was a crude experiment (the field was switched on and off manually). Comparing Figure 13 with Figure 12(b), it also appears as though this may even be an improvement over the initial response (Figure 12(a)). The rise time of the high-voltage diffraction is 12 sec and the decay time 1 sec. The low-voltage diffraction has a rise time of 10 sec and decay time of 2 sec.

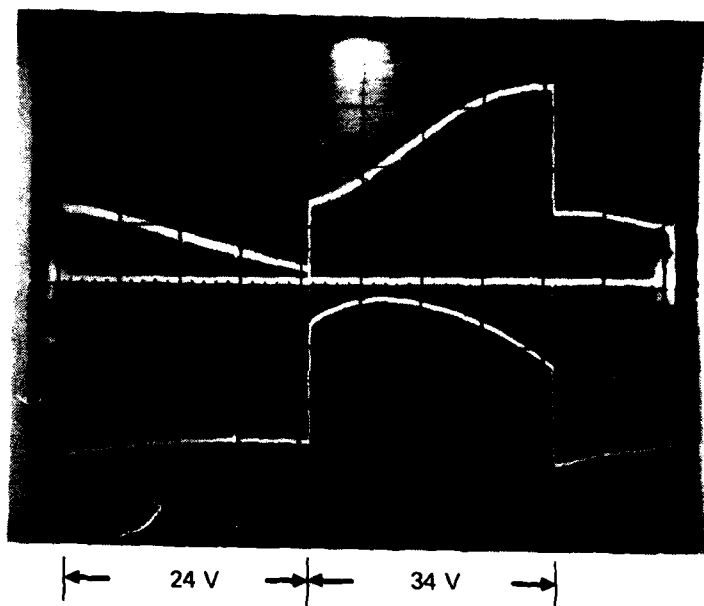
This discovery raises the question of how much response can be improved by using a driving field that is specially shaped for a maximum response. This is a promising area for further experimentation.

#### B. DYNAMIC RESPONSE STUDIES OF VGM USING APPLICATION OF AC AND DC TO IMPROVE RESPONSE SPEED

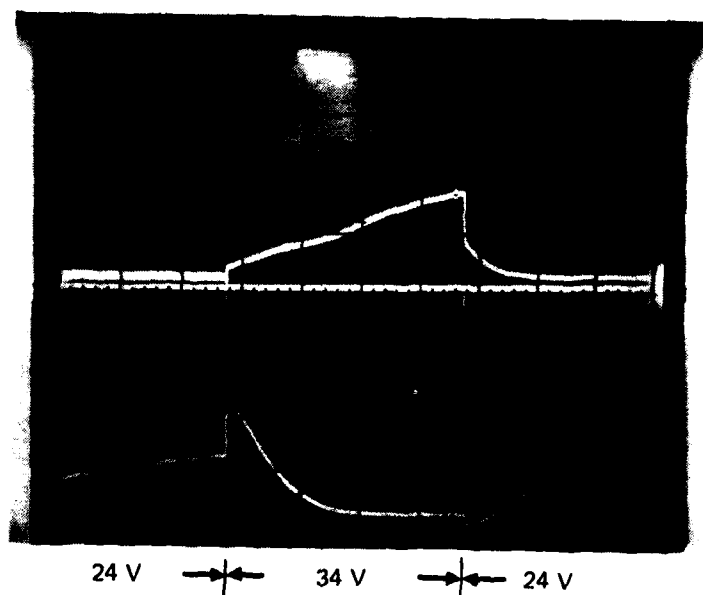
We have studied some of our VGM LCs to determine the effect of combined ac and dc on the speed of observed response. We have also studied an LC with a dielectric anisotropy "crossover" (wherein the anisotropy changes from positive to negative with application of increased frequency) to determine if VGM can be achieved when the necessary negative anisotropy is induced by fields of high frequency. For these tests we used Merck Laboratories Nematic Phase 1085 TNC LC. Negative dielectric anisotropy is defined as

$$\Delta\epsilon = (\epsilon_{\parallel} - \epsilon_{\perp}) < 0 \quad .$$





(a) BEFORE



(b) AFTER

Figure 12. Response before and after 3 hr of continuous use.

11641-5

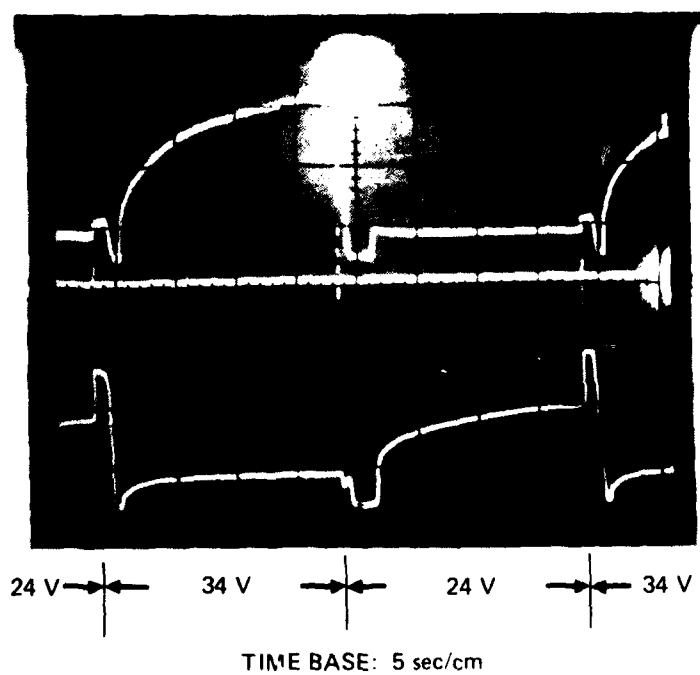


Figure 13. Response time shortening by deliberate switching of the field to zero.

Eight cells were tested in the following series. Some cells were new fabrications, and some were cells still available from earlier tests. The test system consisted of an ac/dc coupling switch to enable application of ac and dc in parallel to the test cell. VGM or optical response was viewed in the cell with a polarizing stereo microscope. The ac field applied was continuously variable in voltage and frequency from 0 to 50 V-ac and 2 Hz to 1 MHz, respectively. The parallel dc field was variable from 0 to 50 V-dc. The full range of frequencies and voltages were applied to the test cells to observe the effects on LC response (see Table 6).

Except for one case where decay response was improved (No. 2), and another where alignment was slightly improved (No. 1), ac generally had the negative effect of suppressing VGM. No VGM has been observed by us by ac alone.



Some experiments were made with HRL-LC 2N40 to determine the effects of varying the amplitude and polarity of the dc fields on the VGM response.

One striking result is illustrated in Figures 14 and 15. There can be an enhancement of the diffraction efficiency by the application of additional short voltage pulses without a change in the diffraction angle. In Figure 14 we see a short flash of scattered light incident upon the detector when the field is switched rapidly from 20 V to -20 V-dc. The decay time follows the short flash.

Some attempts to reduce the delay time were made using a short pulse of dc at a higher voltage than the static level. As can be seen in Figure 15, the pulse actually lengthened the delay time. The power intensity on the detector was greatly increased because of improved diffraction efficiency with the higher field. The starting voltage here is 15 to 50 V-dc for the short pulse; it then returns to 30 V-dc.

As an alternative to the VGM device we are exploring the possibilities of using periodic wedges of birefringent LC to deflect the light electro-optically. In a thin enough structure

Table 6. Combined ac and dc VGM Test Cell Observations

Cell No. and Alignment Type	LC	Thickness	Pin $\Omega$ -cm	DC Threshold, V	AC Threshold	Peak Response Frequency, kHz	10 V-dc Crossover	V-dc	V-dc	Domain Observed	Optical Observations
No. 1 PVA (rubbed)	ZLT1085	1/4 mil	$2.2 \times 10^{11}$	5	15 V	3	7.6 kHz	10	30	Transient (possibly Williams) domains, no VGM.	AC improves alignment best at 70 to 100 kHz. AC tends to inhibit dc response.
No. 2 MAD & SAD S10	ZLT1085	1/4 mil	$8.5 \times 10^{10}$	5	14 V	3	7	10	28	Transient (possibly Williams) domains, no VGM.	Increased dc increases crossover frequency. Decay response improved with ac applied. Alignment may have high tilt angle.
No. 3 PVA (rubbed)	ZLT1085	1/4 mil	$4.4 \times 10^{10}$	8	20 V	2.5	7	16	40	Transient (possibly Williams) domains on VGM	No apparent alignment change with ac applied. None or minor decay response with ac applied.
No. 4 MAD-SAD S10 PARALLEL 	2N40	1/4 mil	$1.45 \times 10^{10}$	14	No response	—	None	—	—	Random domains 45° to cell alignment direction.	AC fields tent to suppress domains caused by dc. No VGM, possible high conductivity.
No. 5 MAD-SAD S10 PARALLEL 	2N40	1/4 mil	$1.66 \times 10^{11}$	13	No response in LC. High current breaks contact.	—	None	—	—	Random domains 45° to cell (possibly Williams).	No VGM, possible high conductivity.
No. 6 PVA (rubbed)	NPV	7.5 $\mu$ m	$1.32 \times 10^{10}$	13	No response. VGM is suppressed at 300 kHz (peak).	VGM is suppressed at 300 kHz	None	—	—	VGM good at threshold and slightly above.	High dc voltage (20 V-dc and up) breaks up VGM into small domains. Probably due to LC deterioration. DSM at edges.
No. K1720-96C PVA	2N40	1/4 mil	$4.0 \times 10^9$	14.6	AC suppresses VGM with peak at 200 kHz. Heats cell raising VGM to 20 V-dc.	VGM with peak at 200 kHz. Heats cell raising VGM to 20 V-dc.	None	—	—	VGM good at threshold and slightly above.	Voltage above 20 V-dc breaks up VGM into small domains. AC improves off-state alignment.
No. 12/1/81 PVA (rubbed)	2N40	7.5 $\mu$ m	$5.9 \times 10^{10}$	16.6	AC suppresses VGM with peak at 300 kHz.	VGM with peak at 300 kHz.	None	—	—	VGM good.	AC has no effect on off-state alignment. VGM good to 50 V-dc.

11641-4

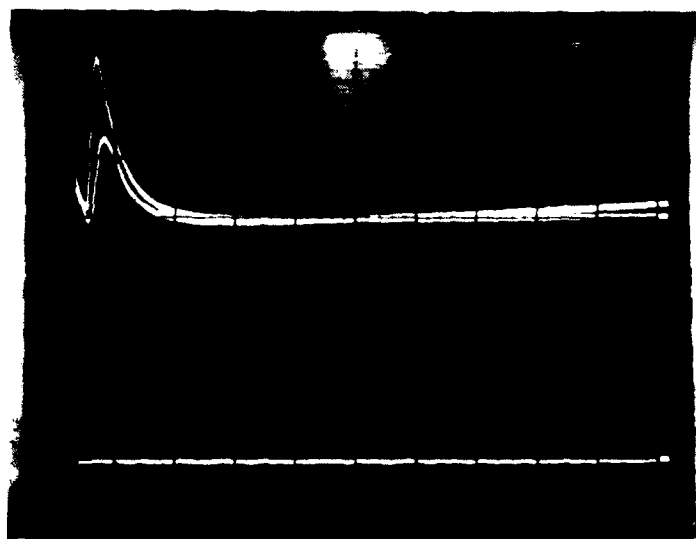


Figure 14. Scattered light impulse  
when switching from 20 to  
-20 V.

11641-3

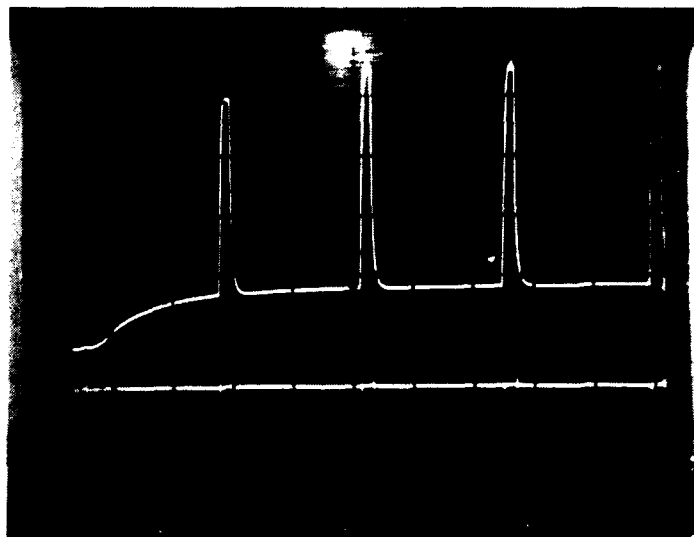


Figure 15. Effect of short superimposed dc pulses on VGM efficiency.

we should expect response times compatible with real time device operation. We are taking two different approaches to realize these structures. In one, we will fabricate on BK-7 glass, a periodic wedge of 200 lines/in. In the second we are attempting to coat some acrylic Fresnel lenses purchased from stock optical supplies. Much difficulty has been encountered in applying transparent conductive coatings to these plastic surfaces, so we are now attempting metal coatings.

Finally, in this period we have worked closely with the USC Image Processing Institute under Professor Sawchuk to measure and model the VGM effect to gain an understanding of the origin of the effect. This will lead to the possibility of altering the LC mixtures to optimize the performance of VGM. From an extensive series of polarization intensity measurements we have been able to deduce that the LC director forms a periodic helical structure in the VGM. The periodic uniaxial birefringence model explains almost all the observations. An in-plane and out-of-plane rotation angle are both specified in the model. There is yet a certain asymmetry in the Jones matrix description of the VGM cell that must be explained before full confidence can be placed in our model.

#### C. IMPROVED VGM RESPONSE SPEED BY SPOILING THE LONG RANGE ORDER

From the device standpoint, the VGM response times, as we have noted before, are too slow for many applications. It would be desirable to have responses compatible with TV frame rates or faster, on the order of tens of milliseconds. In this section we describe a novel approach to, and some preliminary results for, achieving faster dynamic response. It is based on the intuitive notion that the VGM domains evolve slowly in time both along the domain direction and in the perpendicular direction.

There is some visual evidence for the slow evolution of the domains. When the voltage is changed in a VGM cell, say to a slightly higher value, under the polarizing microscope one can see the new additional lines coming into the field of view. New lines

form by "unzipping" one or more of the numerous fork-shaped dislocations which occur throughout the area of the VGM structure. The unzipping process typically traverses  $\sim 20 \mu\text{m}$  at velocity on the order of magnitude  $10 \mu\text{m}/\text{sec}$ .

It seemed possible that if the length of the VGM grating domain could be shortened radically so that the unzipping would not have to travel far, that the time of formation of the new VGM steady state could be shortened. One way to cover a two-dimensional area with short VGM domains would be to have the longer domains interrupted by a fixed set of parallel interruptions perpendicular to the length of the domains. The interruption would have to present a strong electrical and/or mechanical perturbation.

We constructed a special cell with one narrow 1-mm groove parallel and another perpendicular to the VGM domains. No difference in response times was noted between these grooves nor between them and the normal large area VGM cell geometry.

Next we fabricated a set of holographically produced gratings with a  $1 \mu\text{m}$  period. These were formed on ITO coated glass substrates etched through the conductive coating. The conductive strips were all electrically connected at one edge. The LC mixture, Merck NPV, was aligned perpendicular to the direction of the grooves of the holographic grating in those experiments that we will report on here. In another set of experiments with the alignment parallel to the grooves, no significant effects were noted.

The VGM domains in a working cell  $6 \mu\text{m}$  thick with 20 V-dc applied are shown in Figure 16. The domains are perpendicular to the two  $1\text{-}\mu\text{m}$  holographic gratings. In the photograph, that grating cannot be seen, and only large occasional defects along the direction of the grooves show up. What is noteworthy in this typical photograph is the large number of forked dislocations, compared with a cell made of normal substrates without any gratings. The domains, however, are not merely  $1 \mu\text{m}$  long, but typically extend  $\sim 10 \mu\text{m}$  in length.



12545-1



Figure 16. VGM domains aligned perpendicular to the horizontal  $1\text{ }\mu\text{m}$  holographic gratings in a  $6\text{ }\mu\text{m}$  thick cell with 20 V.

To measure the temporal response of this cell, an apparatus similar to that shown in Figure 1 was used. The main difference is that here two detectors were employed. The voltage on the cell was repetitively switched from one dc value to another in a rectangular wave pattern. One detector was placed at each of the diffraction positions appropriate for each voltage. The outputs of these detectors were displayed on dual traces of an oscilloscope. For example, in Figure 17, the top trace records the output of the detector placed at the 30-V diffraction position, while the bottom trace simultaneously records the output of the detector at the 20-V diffraction position as the voltage is repetitively switched from 20 to 30 V with a 2-sec period. The motion of the diffracted light beam from one detector to the other is complex. Not only does the beam travel from one detector to the other, but it also undergoes a reformation and condensation as it approaches steady state, making the temporal response very complicated, as can be seen from the oscilloscope traces. There is also a sudden flash of light, largely centered around the current position, whenever the voltage is switched. This flash shows up as a strong spike on the traces. From Figure 17 we estimate the rise time to be  $600 \pm 200$  msec and the decay time is in the tens of milliseconds! In Figure 18 the cell was refilled, traces were recorded from 30 to 40 V. The top trace corresponds to 40 V. Here the rise times were on the order of 100 msec, but the decay times were 600 and 1,700 msec, respectively, for 30 and 40 V. This was clearly not a reproduction of the remarkable rapid decay observed in Figure 17.

Generally, at this stage in our experiments, we have been able to reproduce the fast performance only from time to time in certain remakes of the cells. However, we are greatly encouraged to have seen this significant improvement in temporal response.

#### D. ALTERNATIVES TO THE VGM DEVICE

Alternatives to the VGM device are being investigated. The essential feature of the VGM device is that it maps local image intensity into spatial positions. The device does this

12545-2

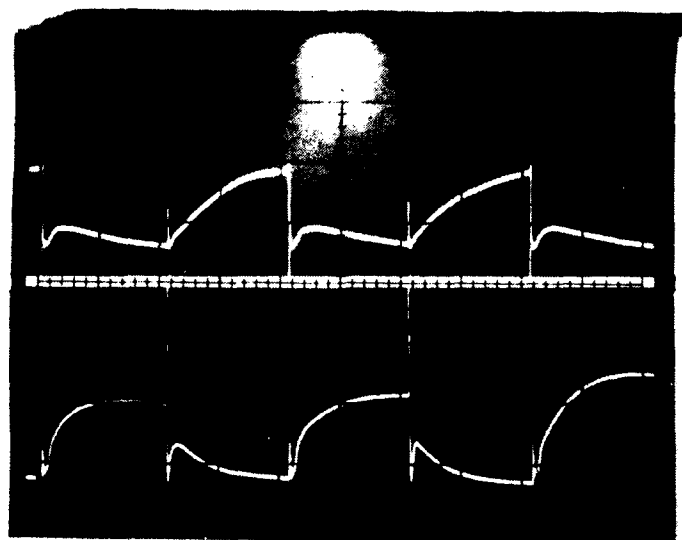


Figure 17. VGM temporal response +20 to +30 V  
1  $\mu$ m grating substrates 500 msec/cm.

12545-3

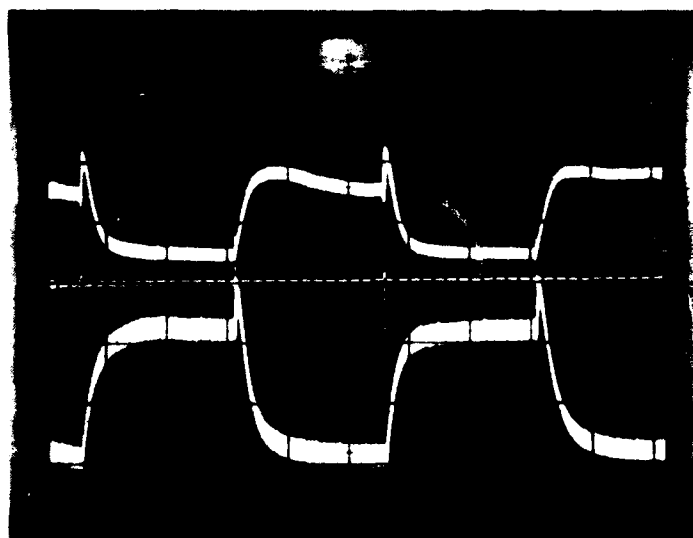


Figure 18. VGM temporal response +30 to +40 V  
1  $\mu$ m grating substrates 2 sec/cm.

very well, but it still has shortcomings — slow response and short degradation lifetime. One alternative device that would preserve the essential feature, yet overcome the present failings, would use the electro-optically induced birefringence change in a LC in wedge or prism-shaped devices. We have performed preliminary experiments to evaluate these ideas. The angle  $\theta$  that light is deflected by refraction from a prism of small angle  $\alpha$  and of index of refraction  $n$  is approximately  $\theta = \alpha n$ . The index of refraction can be varied electro-optically in many materials, and the effect is particularly large in LCs where the change in index  $\Delta n$  between the ordinary and extraordinary polarization can be as much as 0.2 with relatively small voltages,  $\sim 10$  V. The change in the angle of deflection  $\delta\theta$ , caused by a change in the index is given by

$$\delta\theta = \alpha \Delta n .$$

By varying the voltage locally in accordance with a two-dimensional image using a photoconductive layer on top of the wedge, one could in principle, have a device that transforms local image intensities into local angles of deflection. In the back focal plane of a lens, these angles are mapped into displacements, i.e., Fourier transform space with the additional parameter of intensity.

Experiments were performed to test the applicability of a simple prismatic wedge of LC as an electro-optically controllable beam deflector. One-inch pieces of glass were spaced at  $250 \mu\text{m}$  at one end and  $3 \mu\text{m}$  at the other, and were filled with nematic mixture E7 whose birefringence is  $\Delta n = 0.23$ . One piece of glass was coated with an ITO transparent layer, and the other with a reflective layer of aluminum. For convenience the cell was used in reflection, thereby doubling the angle of deflection. AC voltages at approximately  $10^3$  Hz were used. The maximum deflection expected,

$$\delta\theta = 2 \alpha \Delta n = 2(1/100)(0.23) = 4.6 \cdot 10^{-3} \text{ rad} ,$$

was a bit larger than the maximum observed of  $3.1 \cdot 10^{-3}$  rad. Alignment and surface effects explain why only 67% of the

predicted deflection by these very simple considerations, was actually achieved. However, the main problem is the slow time of response of the thick LC. A second problem is the scattering that occurs when the cell is more than 100  $\mu\text{m}$  thick. At the 100  $\mu\text{m}$  thickness, the deflection response times were 2 sec rise time, and 25 sec decay time. Response time is roughly related to the inverse square of the thickness, but one would have to have a very much thinner cell to get responses in the millisecond region.

A potential solution to these problems was invented in this period. Since only the wedge angle determines the deflection of the prism and not the thickness, one could have an array of replicated little prisms that would effect the same deflection without the disadvantages of slow speed and cloudiness caused by a large thickness. Just as in the Fresnel lens, here too, excessive refractive material can be eliminated. Care must be taken in design so that the spacing is not so fine as to be in the diffraction region, and spacing is not so coarse that the height of the prisms is too great.

One attempt at realizing a workable periodic wedge was to use a reflective, conducting, replica-blazed diffraction grating as one element of an LC cell. A blazed grating with a groove profile that is roughly triangular seemed to work well. We used a 600 1/mm, 5,000  $\text{\AA}$  blazed grating, which implied an effective wedge angle of  $8.7^\circ$ . At most, with good alignment, no surface effects, and full birefringence, we could have expected an electro-optic deflection of  $69 \cdot 10^{-3}$  rad but we observed only  $1.2/10^{-3}$  rad. It became clear that using such a fine period grating, where diffraction and refraction compounded their effects, was not practical.

We are now pursuing two different approaches to realize these periodic wedge electro-optic deflectors. We will attempt to fabricate this structure on BK-7 glass substrates at a period of 250  $\mu\text{m}$  and a wedge angle of less than  $45^\circ$  to avoid the problems discussed above. Conventional glass fabrication techniques have proved extremely expensive. An alternative approach we are attempting is to employ structures already fabricated for other

purposes, then adapting them to our needs. For example, plastic replica Fresnel lenses have been purchased and attempts are under way to coat the surfaces with transparent and conductive electrodes. If successfully done, then the power or magnification of these lenses could be negated 1 atm by additional optical elements to achieve the pure deflection that is desired in these experiments. Thus far, we have had great difficulty in applying conductive coatings to acrylic Fresnel lenses using vacuum coating techniques. We have backspattered with a freon etch followed by a flash coat of tantalum.  $\text{SiO}_2$  was then deposited in a oxygen-rich atmosphere followed by ITO, again in oxygen-rich atmosphere. Unfortunately, adhesion to the substrates has been poor and the conductivity is too low. Metallizing the acrylic substrates with paladium-tin or gold, then ion beam etching for LC alignment, has not yet been successful. The alignment has been too random and the coatings have a tendency to peel. Further work is continuing to solve these problems.

### SECTION 3

#### PERSONNEL

The professional personnel associated with this research effort at HRL are Bernard H. Soffer, principal investigator and program manager; Don Boswell; Anna Lackner; and David Margerum.

## SECTION 4

### PUBLICATIONS AND PRESENTATIONS RESULTING FROM AFOSR SUPPORT

#### A. PUBLICATIONS

This section lists written publications from AFOSR support from the initial starting date.

1. A. Armand, D. Boswell, A.A. Sawchuk, B.H. Soffer, and T.C. Strand, "Real-Time Nonlinear Optical Processing with Liquid Crystal Devices," Proceedings 1978 International Optical Computing Conference, London, 153-156 (September 1978).
2. A. Armand, D. Boswell, A.A. Sawchuk, B.H. Soffer, and T.C. Strand, "Approaches to Nonlinear Optical Processing in Real-Time," Proceedings International Commission for Optics Congress, Madrid, Spain, 253-256 (September 1978).
3. A. Armand, D. Boswell, J. Michaelson, A.A. Sawchuk, B.H. Soffer, and T.C. Strand, "Real-Time Nonlinear Processing with Halftone Screens," 1978 Annual Meeting, Optical Society of America, San Francisco, October 1978, J. Opt. Soc. Am. 68, 1361 (October 1978).
4. A. Armand, D. Boswell, A.A. Sawchuk, B.H. Soffer, and T.C. Strand, "New Methods for Real-Time Nonlinear Optical Processing," 1978 Annual Meeting, Optical Society of America, San Francisco, California, October 1978, J. Opt. Soc. Am. 68, 1361 (October 1978).
5. A. Armand, A.A. Sawchuk, T.C. Strand, D. Boswell, B.H. Soffer, "Real-Time Parallel Optical Analog-to-Digital Conversion," Optics Lett. 5, 129-131 (March 1980).
6. B.H. Soffer, D. Boswell, A.M. Lackner, A.R. Tanguay, Jr., T.C. Strand, and A.A. Sawchuk, "Variable Grating Mode Liquid Crystal Device for Optical Processing," Proceedings Society of Photo-Optical Instrumentation Engineers Los Angeles Technical Symposium - Devices and Systems for Optical Signal Processing 218, 81-87, Los Angeles, California, February 1980.
7. B.H. Soffer, D. Boswell, A.M. Lackner, P. Chavel, A.A. Sawchuk, T.C. Strand, and A.R. Tanguay, Jr., "Optical Computing with Variable Grating Mode Liquid Crystal Devices," Proceedings Society of Photo-Optical Instrumentation Engineers Technical Symposium East - 1980, Optical Computing Conference 232, 128-136, Washington, D.C., April 1980.



8. P. Chavel, A.A. Sawchuk, T.C. Strand, A.R. Tanguay, Jr., and B.H. Soffer, "Optical Logic with Variable Grating Mode Liquid Crystals Devices," Optics Lett. 5, 398-400, September 1980.
9. B.H. Soffer, J.D. Margerum, A.M. Lackner, D. Boswell, A.A. Sawchuk, A.R. Tanguay, T.C. Strand, and P. Chavel, "Variable Grating Mode Liquid Crystal Device for Optical Processing and Computing," Molecular Crystals and Liquid Crystals 70, 145-161 (1981).
10. A. Armand, T.C. Strand, A.A. Sawchuk, and B.A. Soffer, "Real-Time Parallel Logarithmic Filtering," Opt Lett. 7, 451-453, September 1982.
11. A.A. Sawchuk, T.C. Strand, and B.H. Soffer, "Intensification Spatial Frequency Transformation in Optical Signal Processing, Proceeding SPIE "Advanced Inst. on Transformations in Optical Signal Processing," (February 1981) to be published.

#### B. ORAL PRESENTATIONS

This section lists oral presentations at meetings and conferences describing research supported by this contract from the initial starting date.

1. A. Armand, D. Boswell, A.A. Sawchuk, B.H. Soffer, and T.C. Strand, "Approaches to Nonlinear Optical Processing with Liquid Crystal Devices," presented at the 1978 International Optic Computing Conference, London (September 1978).
2. A. Armand, D. Boswell, A.A. Sawchuk, B.H. Soffer, and T.C. Strand, "Approaches to Nonlinear Optical Processing in Real-Time," presented at the International Commission for Optics Congress, Madrid, Spain (September 1978).
3. A. Armand, D. Boswell, J. Michaelson, A.A. Sawchuk, B.H. Soffer, and T.C. Strand, "Real-Time Nonlinear Processing with Halftone Screens," presented at 1978 Annual Meeting, Optical Society of America, San Francisco, California (October 1978).
4. A. Armand, D. Boswell, A.A. Sawchuk, B.H. Soffer, and T.C. Strand, "New Methods for Real-Time Nonlinear Processing," presented at 1978 Annual Meeting, Optical Society of America, San Francisco, California (October 1978).

5. A.A. Sawchuk, T.C. Strand, A.R. Tanguay, Jr., P. Chavel, D. Boswell, and B.H. Soffer, "Parallel Optical Analog-to-Digital Conversion Using a Liquid Crystal Light Valve," Workshop on High Speed A/D Conversion, Portland, Oregon (February 1980).
6. B.H. Soffer, D. Boswell, A.M. Lackner, A.R. Tanguay, Jr., T.C. Strand, and A.A. Sawchuk, "Variable Grating Mode Liquid Crystal Device for Optical Processing," presented at SPIE Los Angeles Technical Symposium-Devices and Systems for Optical Processing, Los Angeles, California (February 1980).
7. B.H. Soffer, D. Boswell, A.M. Lackner, P. Chavel, A.A. Sawchuk, T.C. Strand, and A.R. Tanguay, Jr., SPIE Technical Symposium East - 1980 Optical Computing Conference, Washington, D.C. (April 1980).
8. A.A. Sawchuk, T.C. Strand, A.R. Tanguay, Jr., P. Chavel, D. Boswell, A.M. Lackner, and B.H. Soffer, "Variable Grating Model Liquid Crystal Light Valves and Their Application to Optical Processing," Gordon Research Conference on Coherent Optics and Holography, Santa Barbara, California (June 1980).
9. B.H. Soffer, D. Boswell, A.M. Lackner, A.R. Tanguay, Jr., T.C. Strand, and A.A. Sawchuk, "Variable Grating Mode Liquid Crystal Devices for Optical Processing and Computing," Eighth International Liquid Crystal Conf., Kyoto, Japan (June 1980).
10. A.R. Tanguay, Jr., T.C. Strand, P. Chavel, B.H. Soffer, and A.A. Sawchuk, "Theoretical and Experimental Polarization Properties of the Variable Grating Mode Liquid Crystal Structure," presented at Annual Meeting of Optical Society of American, Orlando, FL, Oct. 1981.
11. B. Soffer, "Technical Applications of the Variable Grating Mode Effect," presented at 4th Liquid Crystal Conference, Tbilisi, Georgia, USSR, Sept. 1981.

## APPENDIX

*Mol. Cryst. Liq. Cryst.*, 1981, Vol. 70, pp. 145-161

0026-8941/81/7001-0145 \$06.50/0

© 1981 Gordon and Breach, Science Publishers, Inc.

Printed in the United States of America

# Variable Grating Mode Liquid Crystal Device for Optical Processing and Computing†

B. H. SOFFER, J. D. MARGERUM, A. M. LACKNER and D. BOSWELL

*Hughes Research Laboratories, 3011 Malibu Canyon Road, Malibu, California 90265*

and

A. R. TANGUAY, JR., T. C. STRAND, A. A. SAWCHUK and P. CHAVEL‡

*Image Processing Institute, University of Southern California, Los Angeles, California 90007*

(Received August 12, 1980; in final form November 13, 1980)

Certain nematic liquid crystal mixtures are observed to form a "variable grating mode" (VGM) for appropriate choices of cell design and applied voltage. In this mode of operation, a phase grating in the plane of the cell arises from a periodic variation in the orientation of the liquid crystal director. The grating spatial frequency is observed to vary linearly as a function of the applied voltage above the formation threshold. Liquid crystal and device parameters characteristic of the observed variable grating mode are presented. Utilization of the VGM effect in a photoconductively-addressed device is shown to provide an intensity-to-spatial frequency conversion. Applications of this unique type of optical transducer to arbitrary nonlinear optical processing problems are described. Results of level slicing experiments and implementation of optical logic functions are presented.

## 1 INTRODUCTION

The variable grating mode (VGM) effect, in which some nematic liquid crystal layers exhibit a laterally periodic optical phase characterized by a voltage dependent spatial frequency, has been observed by several authors.<sup>1-6</sup> A VGM liquid crystal device can be constructed with the addition of a photoconductive layer in series with the liquid crystal layer.<sup>4</sup> When utilized as an optical-to-

\*Presented at the Eighth International Liquid Crystal Conference, Kyoto, 1980.

‡Permanent address: Institut d'Optique, Université de Paris sud, Orsay, France.

optical image transducer, this device has the rather unique property of converting in real time the intensity of an input image into a spatial frequency. Such an intensity-to-spatial frequency converter can be employed to implement arbitrary nonlinear point operations on input images.

In section II of this paper, we describe our investigations on the VGM effect as a function of compositional differences in phenyl benzoate liquid crystal mixtures, from which we chose an ester mixture for use in our photoactivated device. The construction and operation of this VGM liquid crystal device is described in section III. The unique approach to real time point nonlinear optical processing offered by this device is illustrated in section IV. The principal advantages with respect to earlier point nonlinear optical processing schemes<sup>1,12</sup> including real time approaches<sup>13,16</sup> are discussed, especially for the implementation of optical binary logic operations.<sup>17,19</sup>

## II VGM EFFECTS AND MATERIALS CONSIDERATIONS

In the variable grating mode operation of liquid crystals, a phase grating is formed with a period that depends upon the voltage placed across the cell. This phase grating originates from a variation of the optical path length due to a periodic orientational perturbation of the liquid crystal uniaxial index ellipsoid. The direction of periodicity is perpendicular to the quiescent state alignment of the liquid crystal molecules, i.e., the domains are parallel to the liquid crystal alignment in the off state. Typical spatial frequency variation is from 100 to 600 cycles/mm. Figure 1 shows typical voltage-induced behavior of a VGM cell as seen through a polarizing microscope. The period of the phase grating can be seen to decrease as the applied voltage increases. Some imperfections in the VGM device can also be observed in the photographs.

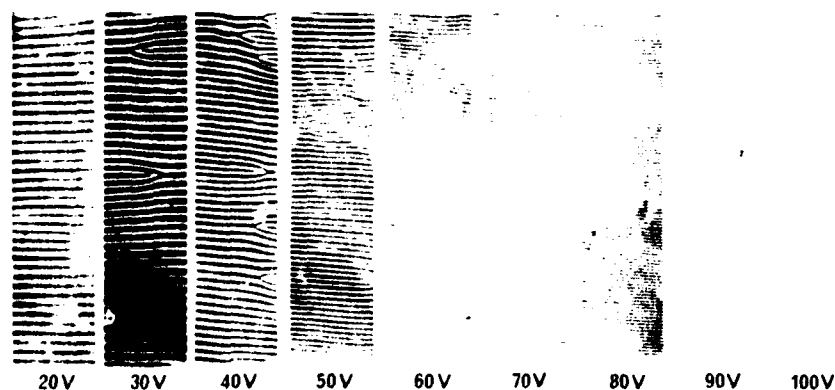


FIGURE 1 VGM viewed through polarizing microscope.

Inconsistencies in the grating alignment within each picture and from picture to picture may be noted. The optical diffraction patterns resulting from the phase grating in a typical VGM cell are shown in Figure 2.

We have observed VGM domains in planar cells up to about  $13\text{ }\mu\text{m}$  in thickness of the liquid crystal. These VGM domains for static fields are always parallel to the quiescent state alignment direction on the electrode surface and are observed only with applied dc fields. These effects are entirely consistent with the experimental results of Barnik *et al.*,<sup>9</sup> but do not support other observations that the cells must be about  $6\text{ }\mu\text{m}$  thick or less,<sup>2,4,5</sup> that the domain can be either parallel or perpendicular to the alignment direction,<sup>2,7</sup> and that ac activation can be used.<sup>2</sup> Our undoped liquid crystals were relatively high in resistivity ( $> 10^{10}\text{ ohm-cm}$ ) and showed little or no dynamic scattering even at dc voltages as high as five times the threshold voltage.

The VGM effect in nematic-phase liquid crystals of negative dielectric anisotropy has been previously studied primarily with azoxy mixtures, such as Merck NP-V. These yellow-colored eutectic mixtures absorb light strongly in the near ultraviolet and blue (below  $430\text{ nm}$ ) region of the spectrum, and can undergo photodecomposition during extended illumination. We studied phenyl benzoate liquid crystal mixtures because they are colorless (strong absorption below  $350\text{ nm}$ ), are more stable to visible light exposures, and are more easily purified than the azoxy mixtures. Since we have been studying structural effects (particularly molecular length) on the anisotropic and dynamic scattering properties of a series of phenyl benzoate mixtures,<sup>21</sup> we ex-

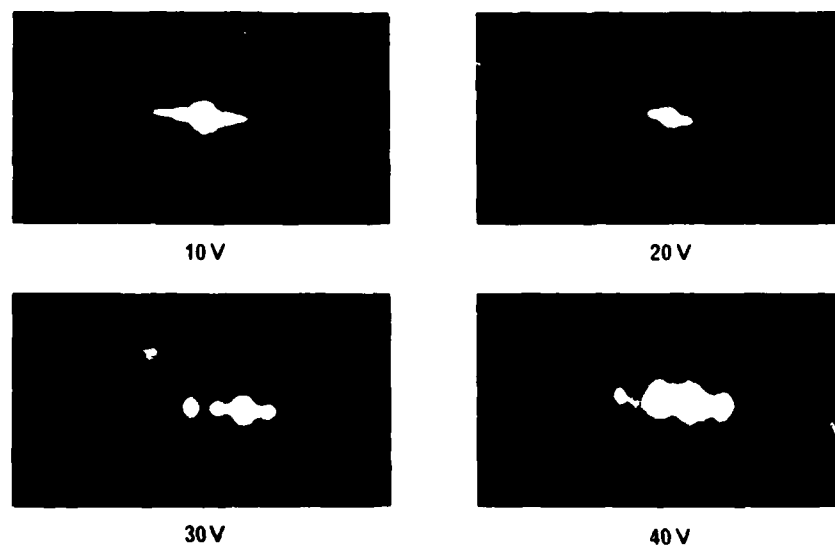


FIGURE 2. Diffraction patterns of a VGM cell.

amined the VGM response of this series as well as several other mixtures. The purpose was two-fold: (1) to select phenyl benzoate mixtures suitable for VGM studies in photoactivated devices, and (2) to look for correlations of structures or physical properties with the VGM effect. The materials studied are shown in Table I. Their VGM characteristics are compared with some of their anisotropic properties in Table II. The voltage dependence of their VGM domain grating frequency is shown in Figure 3.

Typical cells used in the foregoing experiments were fabricated from indium tin oxide (ITO)-coated, 1.27 cm or 0.32 cm thick optical flats. The liquid crystal layer was confined by a 6  $\mu$ m Mylar perimeter spacer. The liquid crystal surface alignment was obtained by spin-coating an aqueous solution containing polyvinyl alcohol on the ITO-coated surfaces, drying at 100°C, and gently rubbing to give a uniform directionality. The effect of dc voltage was observed with a polarizing microscope at 258 $\times$  magnification for each liquid crystal mixture. The width  $d$  of the domain period (line pair) is inversely proportional to applied voltage according to

$$d = \alpha / V \quad (1)$$

where  $\alpha$  is a constant that is dependent on the particular liquid crystal mixture. This relationship is illustrated in Figure 3, in which dc voltage as a function of grating frequency  $1/d$  for each eutectic mixture is a straight line with

TABLE I  
Liquid crystal mixtures used for VGM studies

Class and Number	End Group Composition —Mole Fraction—			Nematic Range		Average Length, Å
	Alkoxy/Alkyl	Dialkoxy	Dialkyl	mp, °C	clpt, °C	
Azoxy						
Merck NP-V	1.000	—	—	—5	73	18.69
RO-R' Esters <sup>a</sup>						
HRL-2N42	1.000	—	—	5	58	20.39
HRL-2N43	1.000	—	—	—6	52	22.37
HRL-2N42/48	1.000	—	—	2	57	23.36
HRL-2N44	1.000	—	—	—8	51	24.31
HRL-2N46	1.000	—	—	16	55	25.92
HRL-2N48	1.000	—	—	18	56	27.14
RO-OR' Components <sup>b</sup>						
HRL-2N11	—	.428	.572	13	47	22.26
HRL-2N40	.755	.245	—	0	58	22.68
HRL-2N25	.772	.228	—	0	56	24.48

<sup>a</sup>RO-R' refers to 4-alkoxyphenyl 4-alkylbenzoate esters. See Ref. 21 for the exact composition of these multicomponent mixtures.

<sup>b</sup>RO-OR' refers to 4-alkoxyphenyl 4-alkoxybenzoate esters. See Refs. 22, 23, and 24 for the exact composition of 2N11, 2N40, and 2N25, respectively. The 2N11 mixture has a R-R' component, 4 butylphenyl 4-toluato, and no RO-R' components.

TABLE II

Liquid crystal anisotropic properties and VGM response

LC Number	Viscosity at 25°C, (cP)	$\Delta n$ at 22°C & 589 nm	AC-Resistivity $\rho_{\perp} \times 10^{-10}$ (ohm-cm)	$\Delta\epsilon$ at 25°C & 5 KHz	$V_{th}$ (volts)	VGM Characteristics <sup>a</sup> Width, $d_{in}$ ( $\mu m$ )	Slope, $\alpha$ (Vmm/lp)
NP-V	24.9	0.290	2.0	-0.2	10	8.5	0.082
2N42	32.6	0.162	6.1	-0.22	10	5.4	0.099
2N43	36.5	0.148	7.2	-0.25	25	8.1	0.287
2N42/48	36.9	0.140	33.0	-0.29	35	5.6	0.340
2N44	38.1	0.136	10.0	-0.30	— <sup>b</sup>	—	—
2N46	39.8	0.135	21.0	-0.30	— <sup>b</sup>	—	—
2N48	44.5	0.134	23.1	-0.33	— <sup>b</sup>	—	—
2N11	43.8	0.133	2.8	-0.5	15	5.1	0.122
2N40	46.9	0.151	8.5	-0.28	16	4.3	0.089
2N25	48.5	0.139	11.0	-0.38	21	7.1	0.203

<sup>a</sup> The threshold voltage,  $V_{th}$ , is the lowest voltage at which the width of the domain period,  $d_{in}$ , was easily measured in cells with 6  $\mu m$  spacers.

<sup>b</sup> No VGM observed up to 100 V dc.

slope  $\alpha$ . Values of  $\alpha$  for various liquid crystal mixtures are given in Table II. A smaller value of  $\alpha$  is preferred, since a smaller slope gives a larger range of spatial frequency for the VGM effect per unit applied voltage. Thus, HRL-2N40 was chosen as the best of these ester liquid crystal mixtures for use in our studies of the photoactivated VGM device. The HRL-2N42 mixture is also of interest because its  $\alpha$  value is almost as low as that of HRL-2N40 and its viscosity is considerably lower.

There is an interesting correlation between the VGM effect and the average

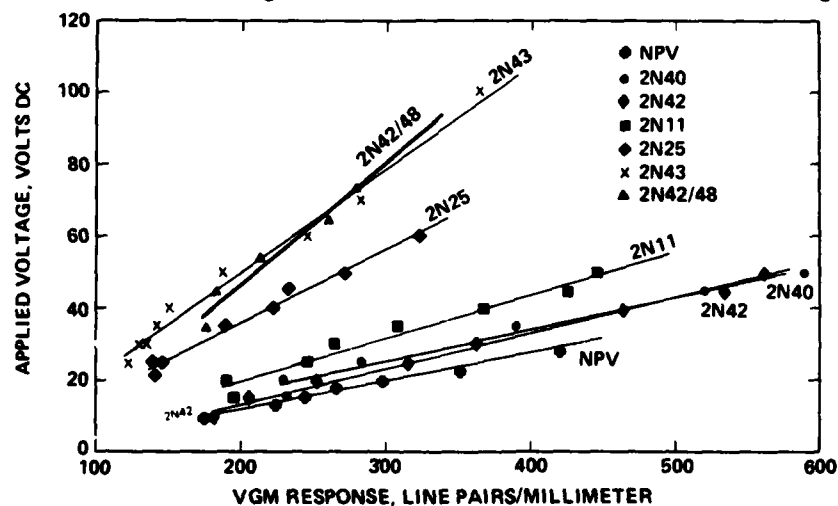


FIGURE 7 VGM voltage dependence for various liquid crystals.

molecular length of the mixtures in the RO-R' ester series in Tables I and II. As their length increases (due to longer alkyl end groups), the  $V_{th}$  and  $\alpha$  of the first three mixtures (2N42, 2N43, and 2N42-48) increase. The longer length mixtures (2N44, 2N46 and 2N48) do not show VGM effects. Since the dielectric anisotropy ( $\Delta\epsilon$ ) is reported<sup>6</sup> to have a large effect on VGM, it may be the change of  $\Delta\epsilon$  with average length that causes these results. In this series the  $V_{th}$  increases as  $\Delta\epsilon$  becomes more negative (with increasing length), and no VGM is observed when  $\Delta\epsilon$  is  $-0.3$  and more negative. This is similar to the VGM effects reported by Barnik *et al.*<sup>6</sup> for a much wider range of  $\Delta\epsilon$ . In a more complex series of phenyl benzoate mixtures (containing four different classes of end groups) they found that  $V_{th}$  increased as  $\Delta\epsilon$  became more negative, and they also reported a critical value of  $\Delta\epsilon = -0.3$ . However, the critical value of  $\Delta\epsilon$  apparently varies with composition of the end group classes used since our 2N25 mixture of RO-R' and RO-OR' esters shows VGM and has  $\Delta\epsilon = -0.38$ . Our latter group of three mixtures (2N11, 2N40 and 2N25), also shows a general trend of increased  $V_{th}$  with more negative  $\Delta\epsilon$ . The effect of  $\Delta\epsilon$  appears to be less significant in these mixtures than in the RO-R' series, but it should be noted that the 2N11 mixture is quite different in composition from the other two mixtures.

The grating lines in the VGM lie parallel to the surface alignment of the liquid crystal director in the off state. Although rubbing has proven to be satisfactory for test cells, a much more uniform homogeneous alignment can be obtained by ion-beam etching certain types of surfaces.<sup>25</sup> Figure 4 shows the best quality of domains that we have thus far obtained.

With the application of alternating fields of about 10 Hz, some cells were conductive enough to exhibit Williams-type domains.<sup>26</sup> These domains are perpendicular to the quiescent state alignment and their periodicity is only slightly affected by the applied field. The Williams domains exist in a narrow range above the threshold voltage due to dynamic scattering resulting from increasing turbulent flow within the cell as the voltage is increased.<sup>27</sup> This effect in conjunction with the very small variation in the spacing of domains, limits the utility of this mode as a diffraction device. For frequencies below 10 Hz, a mixed-mode behavior is observed in the more conductive cells, with VGM and Williams-type domains appearing sequentially. The cells also exhibit severe scattering during the appearance of the Williams domains, especially as the frequency is raised. We have not been able to produce pure VGM behavior with alternating fields of zero average value even for cases of very asymmetric waveforms.

The diffraction efficiency of the VGM cells depends strongly on the applied voltage, and can be as large as 25% in the second order (utilizing HRL 2N40 in a 6  $\mu$ m thick cell). Interesting polarization effects of the odd and even diffraction orders as a function of the input light polarization are being investigated.



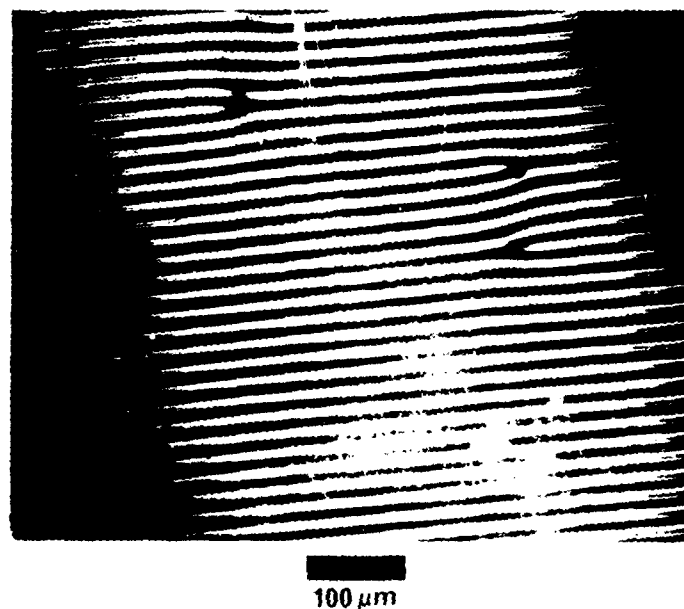


FIGURE 4 The phase grating structure of the VGM device at a fixed voltage viewed through a phase contrast microscope.

### III VGM DEVICE DESCRIPTION

The structure of the present photoactivated VGM device is shown schematically in Figure 5. This configuration is similar to the dc photoactivated liquid crystal devices described previously.<sup>28,29</sup> The cell includes a vapor-deposited ZnS photoconductor and liquid-crystal layer placed between ITO transparent electrodes that have been deposited on glass substrates. In operation, the applied dc voltage is impressed across the electrodes.

The operating principle of the device is straightforward. The photoconductor is designed to accept most of the drive voltage when not illuminated; the portion of the voltage that drops across the liquid crystal layer is below the activation threshold of the liquid crystal VGM effect. Illumination incident upon a given area of the photoconductive layer reduces its resistance, thereby increasing the voltage drop across the liquid crystal layer and driving the liquid crystal into its activated state. Thus, because of the VGM effect, the photoconductor converts an input intensity distribution into a local variation of the phase-grating spatial frequency. The high lateral resistance of the thin photoconductive film prevents significant spreading of the photoconductivity and the associated liquid crystal electrooptic effect. As a result, the light-activation process exhibits high resolution, as will be discussed in more detail below.

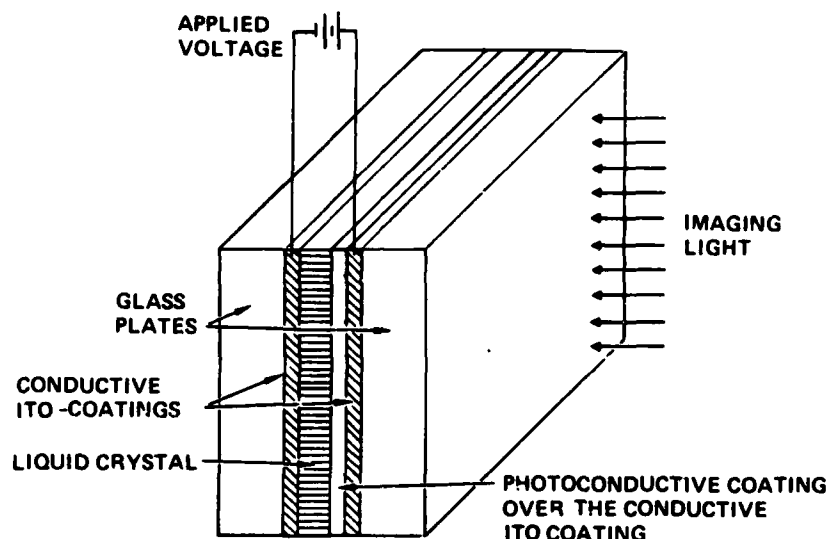


FIGURE 5 Schematic diagram of the VGM device construction. Current devices are read out in transmission at a wavelength at which the photoconductor is insensitive.

Because the VGM phenomenon is a dc instability effect occurring in high-resistivity ( $\rho > 10^{10} \Omega - \text{cm}$ ) pure liquid crystal compounds, the device requires a high resistance photoconductive layer. Zinc sulfide has been selected as the photoconductor material for the best resistance match with the liquid crystal layer. Because the liquid crystal molecules are sensitive to photodecomposition in the ultraviolet, the ZnS layer is preferably made thick enough to optimize photoactivation in the blue region of the spectrum.

The ZnS layer is deposited on transparent ITO electrodes by evaporation or ion-beam-sputtering methods. The sputtered films were  $0.5 \mu\text{m}$  thick, highly transparent smooth surface layers. With the evaporation technique, we produced photoconductors of  $1.5$  to  $5 \mu\text{m}$  thickness, characterized by a hazy, rough surface appearance that caused difficulties in liquid crystal alignment parallel to the electrodes. It has been reported that vaporized ZnS causes homeotropic or tilted homeotropic orientation of the liquid crystal material.<sup>30</sup> Mechanical polishing of the evaporated photoconductors increased their transparency and surface uniformity, while polymer (PVA) coating the top of these ZnS layers, supplemented by additional surface treatment, resulted in good parallel alignment. Photoconductors were evaluated and compared by measuring the dark current and switching ratios of the resulting VGM devices.

From the preliminary photosensitive devices fabricated using a ZnS photoconductive layer to achieve the necessary high resistance, one cell was selected that aligned well and did not suffer the usual rapid deterioration seen in dc

operation. This deterioration is assumed to result from poisoning of the liquid crystal by the diffusion of ions from the photoconductor. This particular cell was constructed of a  $5\text{ }\mu\text{m}$  thick evaporated ZnS layer that had been polished and then rubbed with surfactant polyvinyl alcohol. The counterelectrode was an ITO transparent layer treated with the same surfactant. The  $6\text{ }\mu\text{m}$  thick liquid crystal layer was made of HRL-2N40 ester. The dark series resistance of the  $2.5\text{ cm}$  square cell was measured to be  $3 \times 10^8\text{ }\Omega$ . With  $-160\text{ V}$  applied to the photoconductor electrode and with saturation illumination of  $7.3\text{ mW cm}^{-2}$  in the passband  $410$  to  $550\text{ nm}$ , the spatial frequency of the VGM domains was calculated from the observed angles of diffracted orders to be  $588\text{ lines mm}$ . The device threshold at this illumination was  $21\text{ V}$ , corresponding to a grating frequency of  $103\text{ lines mm}$ . The optical threshold at  $160\text{ V}$  is of the order of  $50\text{ }\mu\text{W cm}^{-2}$ .

Planar VGM test cells were studied with respect to edge effects on resolution and possible "spillover" of domains into adjacent unactivated areas. Electrodes were specially prepared by removing sections of the conductive coating by etching. A parallel plate cell was constructed such that there were conductive areas facing each other, either with conductive edges aligned or with a maximum overlap of  $150\text{ }\mu\text{m}$  of a conductive electrode over the nonconducting area. Cell spacing was  $6.3\text{ }\mu\text{m}$  and the material was Merck NP-V. For alignment parallel to the edge when operating close to the threshold voltage, domains were parallel to the edge and within the active area. For higher voltages, there was fringe spillover by not more than one fringe spacing. For alignment perpendicular to the edge, domains appear to either terminate at the edge or to join with an adjacent domain. The quality of the edge behavior is shown in Figure 6. These studies indicated that implementation of the VGM effect in an image processing device should ultimately produce a resolution not limited by degradation due to edge effects.

#### IV NONLINEAR OPTICAL PROCESSING USING VGM DEVICES

##### IV.A. Implementation of point nonlinear functions

The VGM liquid crystal device can be considered to be an intensity-to-spatial frequency converter capable of operating on two-dimensional images. The intensity-to-spatial frequency conversion allows the implementation of arbitrary point nonlinearities with simple Fourier plane filters. When an input image illuminates the photoconductor surface of this device the intensity variations of the input image change the local grating frequency. If coherent light is utilized to Fourier transform the processed image, different spatial frequency components of the encoded image, corresponding to different input intensities, appear at different locations in the Fourier plane as shown in Figure 7. Within the dynamic range of the device, intensities can thus be mapped

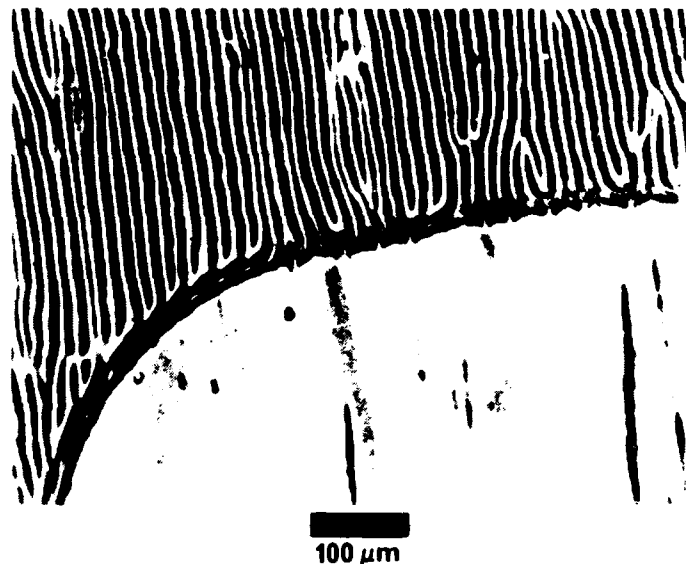


FIGURE 6 Behavior of domains near an edge.

monotonically into positions along a line in Fourier space. The input intensity distribution has thus been coded into Fourier (spatial frequency) space. If the spatial frequencies of the VGM domains are much larger than the largest spatial frequency component encountered in the images to be processed, we are in the tractable situation, familiar in communications theory, where the carrier frequency is much higher than the modulation frequencies. Thus, by placing appropriate spatial filters in the Fourier plane it is possible to obtain different transformations of the input intensity in the output plane as depicted in Figure 7b. This figure describes the variable grating mode nonlinear processing algorithm graphically. The input intensity variation is converted to a spatial frequency variation by the characteristic function of the VGM device (upper right-hand quadrant). These variations are Fourier transformed by the optical system and the spectrum is modified by a filter in the Fourier plane (upper left-hand quadrant). Finally, a square-law detection produces the intensity observed in the output plane (lower left-hand quadrant). Considered together, these transformations yield the overall nonlinearity (lower right-hand quadrant). Design of a proper spatial filter for a desired transformation is a relatively easy task. For example, a level slice transformation requires only a simple slit that passes a certain frequency band or bands. A mathematical formulation of nonlinear processing utilizing the VGM device is presented elsewhere.<sup>31</sup> The principal result of this analysis is the relation

$$h\nu_0 \geq 2N \quad (2)$$

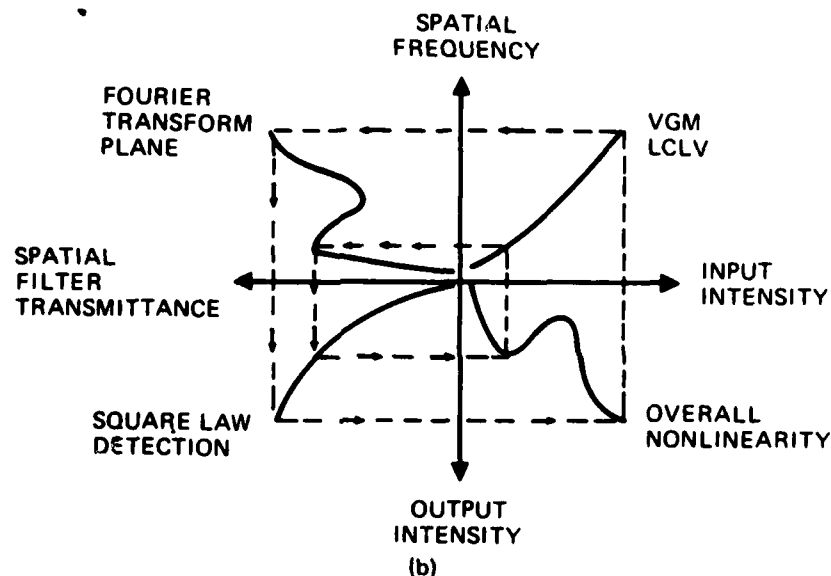
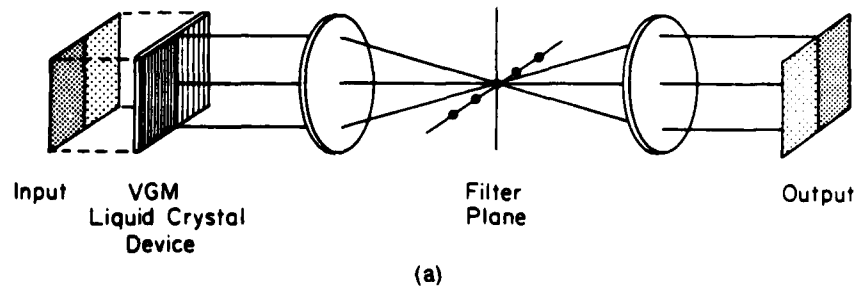


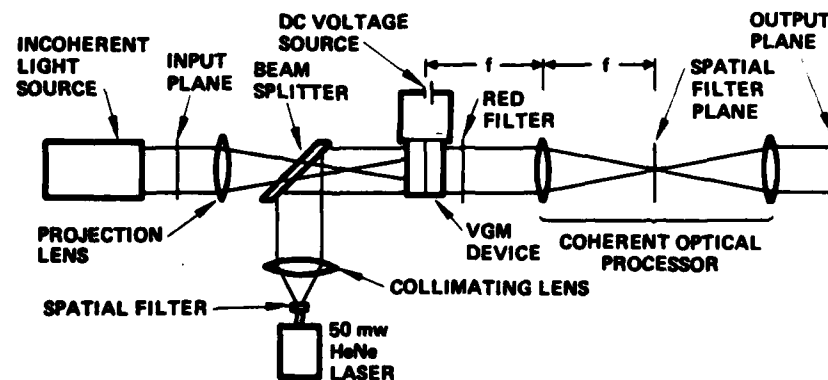
FIGURE 7 VGM nonlinear processing. (a) Experimental setup indicating the mapping of intensity to spatial frequency. (b) The overall input-output characteristic can be found by stepping through the successive nonlinear transformations including (1) the intensity to spatial frequency conversion, (2) spatial filtering, and (3) intensity detection.

where  $h$  is the pixel width,  $\nu_0$  is the lowest usable VGM spatial frequency, and  $N$  is the number of distinguishable grey levels. This relation requires that the pixel size contains  $2N$  periods of the lowest grating frequency if  $N$  grey levels are to be processed. For example, a  $100 \times 100$  pixel image could be processed with 50 distinguishable grey levels on a 50 mm square device with  $\nu_0 = 200$  cycles/mm.

The ability to perform arbitrary point nonlinearities over two-dimensional images greatly increases the flexibility of optical processing system. In the past few years several different approaches to the problem of implementing gener-

The same programmability advantage applies to the implementation of binary logic operations. One device can be used to implement any of the combinatorial logic operations (AND, OR, XOR, and their complements) by simply changing a Fourier plane filter. Previously described optical logic systems were "hardwired" to perform specific operations,<sup>17-20</sup> in most cases one or more logic functions proved difficult or cumbersome to implement. Use of the VGM liquid crystal device for the implementation of combinatorial logic operations is described below.

In this experiment the ability of the VGM device to generate a level-slice non-linearity is demonstrated. The experimental arrangement is shown in Figure 8. A continuous tone input picture is illuminated by an arc lamp source and imaged onto the photoconductor surface of a VGM device which initially exhibits a uniform phase grating structure due to a dc bias voltage. The grating period is locally modulated by the input picture intensity, and this modulation is mapped into a position along a line in the spatial filter plane. A red filter ensures that only the readout laser beam enters the coherent optical processor.



64

Sectors of small circular annuli of varying radii are used to pass certain spatial frequency bands. This in effect allows only prescribed input intensity ranges to appear in the output. Circular rather than straight slits are used to capture the weak light which in small part is diffracted into circular arcs (see Figure 2) because of the grating imperfections (see Figure 1). Figure 9 shows both the input and level sliced output pictures. Figure 9a shows a positive print of the original image as photographed on the imaging screen. A negative of the original was used in the experiments. Figure 9b shows a low intensity level slice corresponding to a VGM spatial frequency of 120 lines/mm with approximately 3% bandwidth. In Figure 9c another level, corresponding to 153 lines/mm, is shown. Figure 9d at 236 lines/mm illustrates the interference from second harmonics. Weak second harmonics of the low intensity image slice corresponding to 118 lines/mm can appear in the 236 lines/mm level slice. In Figure 9e, a broader slice of approximately 11% bandwidth was taken centered about the level corresponding to 140 lines/mm. This picture may be compared with the previous slices and particularly with the slice shown in Figure 9c. Finally, Figure 9f shows a very high input intensity slice at 440 lines/mm with 10% bandwidth. Three grey levels may be seen simultaneously; these correspond to the superposition of three broad intensity slices.

#### IV.C. VGM Implementation of logic functions

To see how the VGM device can be used to implement binary logic operations, one need only realize that the function of a logic circuit can be represented as a simple binary nonlinearity operating on the incoherent superposition of two

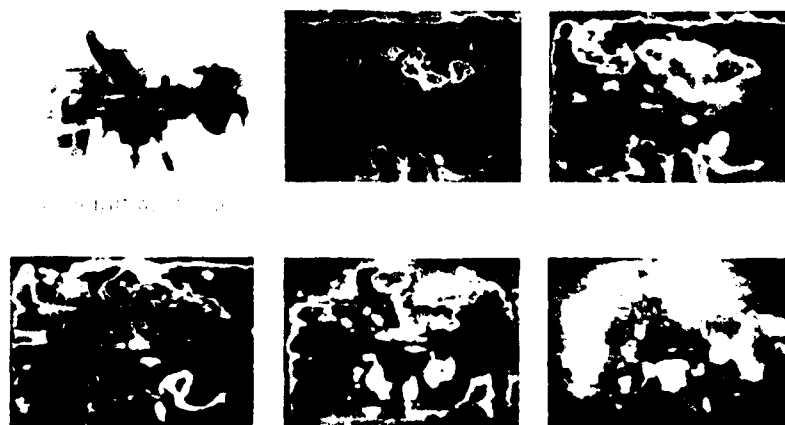


FIGURE 9 Level slice results. (a) Original image b-f) Level slice results for various apertures as discussed in the text.

binary images as input. As shown in Figure 10, NOT is simply a hard-clipping inverter, while AND and OR are hardclippers with different thresholds and XOR is a level slice function.

The VGM device is well suited to implementing this type of nonlinearity. Since the nonlinearities associated with logic operations are binary functions, they can be implemented with simple slit apertures, i.e., 0 or 1 transmittance values. A noteworthy advantage of the VGM approach over previous optical logic methods<sup>17-20</sup> is the ease of programming the nonlinearity, by merely changing the aperture in the spatial frequency plane.

Another feature of the VGM technique that is especially suitable for logic processing is that the input and output are physically separate beams. The input beam modulates a photoconductor; concurrently the image is read out with a second beam. This separation of input and output provides for the possibility of restoring the output levels to the desired 0 and 1 values even if the input levels are not exactly correct. This feature is essential to the production of a reliable logic system that is immune to noise and systematic errors in the levels. Electronic logic elements possess such level restoring capability, but currently proposed optical logic schemes<sup>17-20</sup> lack this essential characteristic.

A series of experiments were conducted to demonstrate the fundamental logic functions. Two input fields were superimposed at the VGM plane along with a bias illumination. The total illumination intensity on the photoconductor of the VGM device was thus the sum of the two input intensities and the bias intensity. The input illumination was filtered high-pressure mercury arc lamp. The bias illumination was provided by a collimated tungsten bulb source. The VGM device was read out in transmission using a HeNe laser. A

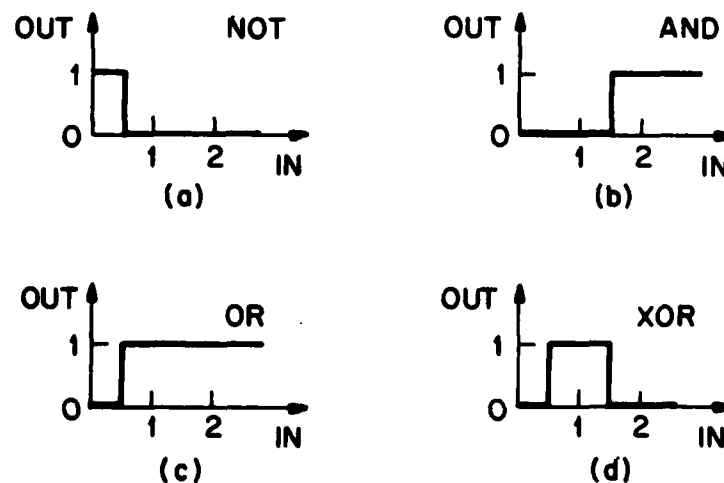


FIGURE 10 Logic functions as simple nonlinearities. Given an input consisting of the sum of two binary inputs, different logical operations can be effected on those inputs by means of the depicted nonlinear characteristics. (a) NOT, (b) AND, (c) OR, (d) XOR.



filter was placed in the Fourier plane to select the desired spatial frequencies for each logic function.

For these experiments, the inputs consisted of one vertical rectangular aperture and one horizontal aperture. When these were superimposed along with the bias, a square image was formed with the four quadrants having the intensity levels shown in Figure 11. This image corresponds to the logic truth table

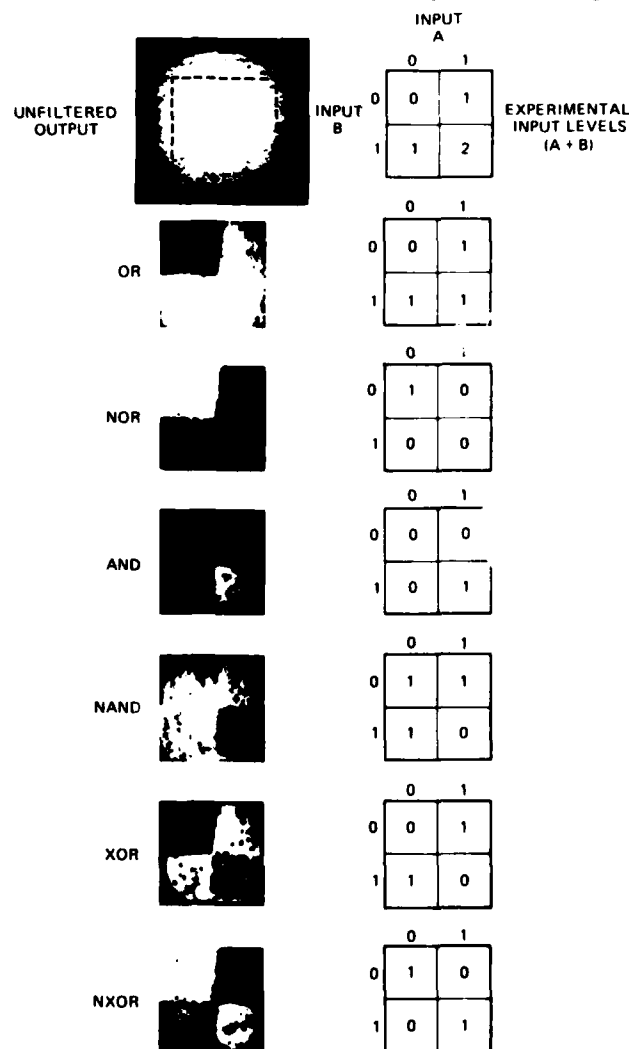


FIGURE 11 VGM logic results. The right-hand column indicates ideal output levels for an image consisting of four quadrants corresponding to truth table values. The left-hand column shows the corresponding experimental results. The first row shows the input for all experiments which consisted of a superposition of two binary images. Succeeding rows show results for the logic operations OR, NOR, AND, NAND, XOR, and NXOR, respectively.

shown. Thus the output images have intensity levels determined by the truth table associated with the desired logic function. The logic functions AND, OR, XOR and their complements were implemented sequentially as shown in Figure 1' by altering only the Fourier plane filter. Imperfections visible to the output plane data arise from defects in the cell structure of the VGM device employed in these experiments.

A more complete discussion of VGM logic implementation can be found in Ref. (32).

## V CONCLUSION

The variable grating mode effect can be incorporated in a photoconductively-addressed device structure which provides an overall intensity-to-spatial frequency conversion. The optical processing experiments using the VGM liquid crystal device described in this paper demonstrate the potential of this real time optical image transducer for numerous parallel nonlinear operations on images. The molecular origin of the VGM phenomenon is now being studied in connection with the behavior of the VGM phase grating as observed by polarization microscopy and polarization-dependent optical diffraction. Improvements in such characteristics of the device as response time, uniformity, dynamic range and density of defects are under continuing investigation.

## Acknowledgments

We gratefully acknowledge the helpful contribution of M. Piliavin in the early phase of this work. This project was sponsored by the Air Force Office of Scientific Research under Grant AFOSR-77-3285 at USC and Contract F49620-77-C-0080 at HRL. Liquid crystal work on the project was partially supported by the Air Force Office of Scientific Research on Contract F49620-77-C-0017 at HRL.

## References

1. L. K. Vistin', *Sov. Phys. Dokl.*, **15**, 908 (1971).
2. W. Greubel and W. Wolf, *Appl. Phys. Lett.*, **19**, 213 (1971).
3. J. M. Pollack and J. B. Flannery, in *Liquid Crystals and Ordered Fluids*, J. F. Johnson and R. E. Porter, eds. (Plenum Press, New York, 1978), **2**, 557.
4. J. M. Pollack and J. B. Flannery, *Society for Information Display 1976 Intern. Symp. Digest*, **143** (1976).
5. P. K. Watson, J. M. Pollack and J. B. Flannery, in *Liquid Crystals and Ordered Fluids*, J. F. Johnson and R. E. Porter, eds. (Plenum Press, New York, 1978), **3**, 421.
6. M. I. Barnik, L. M. Blinov, A. N. Trufanov and B. A. Umanski, *J. de Physique*, **39**, 26 (1978).
7. H. Kato and J. W. Goodman, *Appl. Opt.*, **14**, 1813 (1975).
8. T. C. Strand, *Opt. Commun.*, **15**, 60 (1975).
9. S. R. Dashiell and A. A. Sawchuk, *Appl. Opt.*, **16**, 1009 (1977).
10. S. R. Dashiell and A. A. Sawchuk, *Appl. Opt.*, **16**, 2279 and 2394 (1977).
11. B. J. Bartholomew and S. H. Lee, *Appl. Opt.*, **19**, 201 (1980).

12. A. Tai, T. Cheng and F. T. S. Yu, *Appl. Opt.*, **16**, 2559 (1977).
13. D. Casasent, *Opt. Eng.*, **19**, 228 (1974).
14. S. Iwasa and J. Feinleib, *Opt. Eng.*, **13**, 235 (1974).
15. A. Armand, A. A. Sawchuk, T. C. Strand, D. Boswell and B. H. Soffer, *Opt. Lett.*, **5**, 129 (1980).
16. J. D. Michaelson and A. A. Sawchuk, *Proc. Soc. Photo Opt. Instrum. Engin.*, **218**, 107 (1980).
17. R. A. Athale and S. H. Lee, *Opt. Eng.*, **18**, 513 (1979).
18. S. A. Collins, Jr., U. H. Gerlach and Z. M. Zakman, *Proc. Soc. Phot. Opt. Instrum. Eng.*, **185**, 36 (1979).
19. D. H. Schaefer and J. P. Strong, III, *Proc. IEEE*, **65**, 129 (1977).
20. L. Goldberg and S. H. Lee, *Appl. Opt.*, **18**, 2045 (1979).
21. J. B. Margerum, J. E. Jensen and A. M. Lackner, *Mol. Cryst. Liq. Cryst.* (in press).
22. A. D. Jacobson, *Development of a Reflective Mode Liquid Crystal Light Valve*, NAVSEA Contract N0024-73-C-1185 Final Report (May, 1975).
23. H. S. Lim and M. J. Little, USP 4,128,312 (Dec. 5, 1978).
24. J. D. Margerum, *Anisotropic and Electro-Optical Effects in Liquid Crystals*, AFOSR Contract N49620-77-C-0017 Final Report, (March 1981).
25. M. J. Little, H. L. Garvin and L. J. Miller, in *Liquid Crystals and Ordered Fluids*, J. F. Johnson and R. E. Porter, eds. (Plenum Press, New York, 1978) **3**, 497.
26. R. Williams, *J. Chem. Phys.*, **39**, 384 (1963).
27. G. H. Heilmeyer, L. A. Zanon and L. A. Barton, *Proc. IEEE*, **56**, 1162 (1968).
28. J. D. Margerum, J. Nimoy and S. Y. Wong, *Appl. Phys. Lett.*, **17**, 51 (1970).
29. J. D. Margerum, T. D. Beard, W. P. Bleha and S. Y. Wong, *Appl. Phys. Lett.*, **19**, 216 (1971).
30. H. Kruger, H. F. Mahlim and W. Rauscher, U.S. Pat. 4, 112, 157, September 1978.
31. B. H. Soffer, D. Boswell, A. M. Lackner, P. Chavel, A. A. Sawchuk, T. C. Strand and A. R. Tanguay, Jr., *Proc. Soc. Photo-Opt. Instrum. Eng.*, **232**, 128 (1980).
32. P. Chavel, A. A. Sawchuk, T. C. Strand, A. R. Tanguay, Jr. and B. H. Soffer, *Opt. Lett.*, **5**, 398 (1980).

